

FIR and C⁺ emissions of spiral galaxies disks.

The example of NGC 6946.

S. Sauty¹, M. Gerin^{2,1}, F. Casoli¹

¹ DEMIRM, Observatoire de Paris, 61 Av. de l'Observatoire, 75014 Paris, France; and URA 336 du CNRS

² Radioastronomie Millimétrique, ENS, 24 Rue Lhomond, 75231 Paris Cedex 05, France; and URA 336 du CNRS

Received 15 October 1997; accepted 25 May 1998

Abstract. We present numerical simulations of radiative transfer in the spiral galaxy NGC 6946. The interstellar medium is represented as a two phases medium, with molecular clouds and a smooth diffuse phase. The molecular gas distribution is calculated in a self-consistent way from the distribution of an ensemble of molecular clouds evolving in the gravitational potential of NGC 6946. We simulate star formation by creating OB associations in molecular clouds. The transfer of UV radiation is calculated in the clumpy interstellar medium, to determine the local UV illumination of molecular clouds. We compute the emergent intensity in the UV continuum (912 – 2000 Å), in the H α and C⁺ $^2P_{3/2} - ^2P_{1/2}$ lines as well as in the continuum at far infrared wavelengths, 60, 100 & 200 μ m.

It is possible to obtain a consistent picture of this galaxy with a global star formation rate of 4 M $_{\odot}$ yr⁻¹ (for stars with masses in the range 2-60 M $_{\odot}$) occurring mostly in the spiral arms. The close spatial association of massive stars and molecular clouds has a profound impact on the transfer of UV radiation in the galactic disk and on the dust emission. The median distance travelled by UV photons is about 120 pc. However, when they have escaped from the vicinity of their parent OB associations, UV photons may travel quite far in the disk, up to 1 kpc. The UV opacity of the model spiral galaxy disk, observed face-on, is 0.8 at 1000 Å and 0.7 at 2000 Å.

For radii less than 4 kpc, the C⁺ 158 μ m line is mostly produced in photodissociation regions at the surfaces of molecular clouds. The C⁺ emission from diffuse atomic gas accounts for about 20% of the total. It becomes significant at large distance from the nucleus ($r \geq 4$ kpc). Molecular clouds and diffuse atomic gas have almost equal contributions to the total far infrared emission from 60 to 200 μ m. As a whole, 72% of the 60 – 200 μ m FIR emission can be attributed to dust grains heated by the UV radiation of massive stars and 28% by the radiation field

of the old stellar population.

Key words: Galaxies : ISM, Galaxies : individual: NGC 6946, – ISM : molecules, ISM : dust

1. Introduction

Because the peak of the thermal dust emission occurs in the far-infrared (60-200 μ m) for Galactic interstellar clouds, this wavelength domain is recognized as a very important ‘window’ to study the interstellar medium, both in the Milky Way and in external galaxies. However, due to the lack of spatial resolution provided by telescopes operating at these wavelengths, the interpretation of the signals measured in external galaxies is still a subject of controversy. The debate is focussed on the origins of the heating of dust grains and of the $^2P_{3/2} - ^2P_{1/2}$ C⁺ line at 158 μ m. This fine structure line of ionized carbon is one of the main cooling lines of neutral atomic gas (Wolfire et al. 1995), but it is also seen in HII regions, with different excitation mechanisms in these two cases. Other sources of C⁺ emission are the dense photodissociation regions (PDRs) where intense UV radiation from massive stars impinges on molecular clouds. In these regions, the photodissociation of carbon monoxide creates a layer of ionized carbon at the edge of the molecular cloud, which is a source of intense C⁺ emission.

The far infrared emission is produced by dust grains heated by star light but the relative contribution of young massive stars on one hand, and of the bulk of the stellar population on the other hand, are still debated (see e.g. Walterbos & Greenawalt 1996, Devereux & Young 1990, Cox & Mezger 1989, Thronson et al. 1990, Rice et al. 1990). Using low resolution data from IRAS, IR colors have been used to assess the respective roles of star

forming regions and cirrus in external galaxies at a global scale (e.g. Calzetti et al. 1995). It is difficult to find spiral galaxies dominated by a single population of heating sources, since the relative contributions of massive stars and of the disk population vary from galaxy to galaxy, and probably from place to place in a given galaxy. A main problem of these studies is the lack of spatial resolution at far infrared wavelengths. Even when it is possible to use high spatial resolution data at millimeter and sub-millimeter wavelengths, the gap in spatial resolution from the local interstellar clouds to external galaxies is huge: for nearby galaxies located at distances D of a few Mpc, a one arcmin beam encompasses $0.3(D/1\text{Mpc})\text{kpc}$, much larger than the size of a single molecular complex in the Galaxy, whereas structures down to 0.01 pc are commonly observed in local clouds (Falgarone et al. 1992) and in the Magellanic Clouds (Rubio et al. 1993).

Numerical simulations provide a way out of this problem: it is possible to reproduce the observed molecular gas distribution of nearby spiral galaxies with numerical simulations using observed data as input parameters. For example Garcia-Burillo et al. (1993) were able to fit the spatial distribution and kinematics of the molecular gas in M 51 using the cloud collision code developed by Combes & Gerin (1985). Though this code has a spatial resolution of a few hundred parsecs (the cell size for the large scale dynamics), it is possible to include "micro-physics" at the parsec scale inside each cell. We have taken this approach and implemented star formation in this code to study the far infrared and C⁺ emissions in the spiral galaxy NGC 6946. The next section summarizes the current data on NGC 6946. We describe the model in Sect. 3 and present the results for NGC 6946 in Sect. 4. The implications of this work for the interpretation of the C⁺ and FIR emission of spiral galaxies are discussed in Sect. 5.

2. NGC 6946

NGC 6946 is a nearby Scd galaxy with a low inclination, $i = 34^\circ$ (Considère & Athanassoula 1988). At the adopted distance of 5 Mpc, 1 arcmin on the sky corresponds to a linear size of 1.5 kpc. The main characteristics of NGC 6946 are summarized in Table 1. It shows a weak bar (Martin 1995) and a prominent spiral structure with both an $m = 2$ and an $m = 4$ pattern (Considère & Athanassoula 1988). With this open spiral structure, the arm and interarm regions are resolved at moderate spatial resolution ($30''$). The gas distribution is well known since NGC 6946 has been mapped at high spatial resolution in HI (Boulanger & Viallefond 1992), and CO (Casoli et al. 1990, Clausset et al. 1991). Figure 1 presents a CO(2-1) map obtained at the IRAM 30m telescope (Clausset et al. 1991), and Fig. 2 a V-I color map obtained at the Observatoire de Haute-Provence (OHP) (P. Boissé, private communication). NGC 6946 is marginally resolved in the far infrared maps obtained by IRAS and the KAO (Engar-

giola 1991). It also belongs to the normal galaxy sample studied by ISO and as such has been extensively mapped in the mid and far infrared (Malhotra et al. 1996, Helou et al. 1996, Lu et al. 1996, Tuffs et al. 1996). NGC 6946 is forming stars actively, as revealed by its bright H α emission (Bonnarel et al. 1988a, 1988b, Kennicutt 1989) and the numerous supernovae (Li & Li 1995). Madden et al. (1993) have mapped the C⁺ 158 μm emission at $45''$ resolution with the KAO. Bright C⁺ emission is found in the nucleus and in the disk. At this scale, the C⁺ emission is correlated with the CO emission in the spiral arms and with the HI emission in the outer disk.

3. A model of NGC 6946

3.1. Representation of the interstellar medium.

We have chosen to include two phases for the interstellar medium :

- i) a dense molecular phase composed of spherical molecular clouds with masses ranging from 10^3 to $10^6 M_\odot$ and mean density $50 \text{ H}_2 \text{ cm}^{-3}$. This mean density is used to determine cloud sizes from their masses. The half power width of the molecular layer, defined as $\langle z^2 \rangle^{1/2}$, is equal to 65 pc. The global volume filling factor of this molecular phase in the disk, $\Phi_V(\text{H}_2)$, amounts to 2.5%. The clumpy structure of molecular clouds is taken into account by using a larger density, $5 \times 10^3 \text{ H}_2 \text{ cm}^{-3}$, to compute the C⁺ emission. The C⁺ emission is not sensitive to the gas density when it is larger than $\sim 10^3 \text{ cm}^{-3}$ (see Tielens & Hollenbach 1985 and Sect. 3.6). Indeed, C⁺ observations of nearby molecular clouds show that C⁺ emission is detected over the whole projected surface of molecular clouds (Jaffe et al. 1994). The total mass of dense molecular gas in the model is set to match the value deduced from CO(1-0) observations with a conversion factor of $2.3 \times 10^{20} \text{ H}_2 \text{ cm}^{-2} (\text{K km s}^{-1})^{-1}$, $2.0 \times 10^9 M_\odot$ (Table 1).
- ii) a neutral diffuse phase, with a nearly constant HI density. We have adjusted the value of the mean HI density using the data from Boulanger & Viallefond (1992): it varies slowly from 0.8 H cm^{-3} at the center to 2 H cm^{-3} in the outer disk ($r \sim 6 \text{ kpc}$). We have assumed that the HI disk has a vertical thickness of $360 \text{ pc} = 2H_z$, and that the density is uniform from $-H_z$ to $+H_z$. The velocity dispersion of the diffuse gas is set to 10 km s^{-1} . The total mass of diffuse neutral gas inside a radius of 6 arcmin is taken from the HI observations to be $2.6 \times 10^9 M_\odot$.

In addition to these two phases, we take into account the formation of HII regions around OB associations (see below). For the numerical calculations, we represent the galaxy disk as a large 3D grid. The total grid length L and the cell size r_{cell} are chosen to match the following constraints:

- the grid size has to be at least as large as the optical disk, which has a diameter of 12.5 kpc, in order to be able to follow the path of photons in the external regions of the

galaxy, and the heating of the neutral gas at large distance from the nucleus.

– the spatial resolution, r_{cell} , should be good enough to describe the clumpy structure of the medium: in particular the smallest clouds in the ensemble should occupy at least one cell. With the adopted parameters for the clouds, the radius of the smallest clouds with a mass of $10^3 M_\odot$ is 4.5 pc. This number is only an estimate of the actual size of a given cloud. It is possible to use an alternative method based on the scaling relations for molecular clouds, the so-called Larson’s laws. Using the mass-radius relation $M(M_\odot) = 100R^2(\text{pc}^2)$ (Falgarone et al. 1992), the radius of a $10^3 M_\odot$ cloud is then 3 pc. Another constraint on the spatial resolution is provided by the size of OB associations, which is generally larger than 30 pc (Garmany 1994) and their distance from molecular clouds. Leisawitz (1991) has estimated the mean distance between OB associations and their parent cloud to be about 50 parsecs.

We have chosen as the best compromise to represent the galaxy with a $1024 \times 1024 \times 24$ cell structure. The galaxy size is then $L = 2 \times R_{max} = 12.5$ kpc and the resolution $r_{cell} = 12.2$ pc. The cells are filled with neutral atomic gas, or with molecular gas at the molecular cloud positions, an $10^6 M_\odot$ molecular cloud then occupies $3 \times 3 \times 3$ cells. Finally, we include the ionized gas in the Strömgren spheres centered on each OB association, and replace the molecular and atomic gas with ionized gas whenever required. The radii of the Strömgren spheres are calculated assuming classical ionization in HII-bounded HII regions (Miller & Cox 1993). Because of the coarse spatial resolution of the dynamical code (200 pc), we do not attempt to reproduce the interstellar medium in the central region of NGC 6946 ($r < 500$ pc).

3.2. Spatial distribution of molecular clouds

This section of the code uses the cloud-cloud collision code described by Combes & Gerin (1985), and used by Garcia-Burillo et al. (1993) and Gerin et al. (1991) to model the gas dynamics in nearby galaxies. The molecular clouds move in the gravitational potential of the galaxy, they grow through cloud-cloud collisions, which are sticky processes, and are disrupted by simulated SN events. The molecular gas is immediately recycled into small molecular clouds. The gravitational potential is deduced from an R band image of NGC 6946 (Viallefond & Bonnarel, private communication, Bonnarel et al. 1988), with foreground stars removed. The image has been rotated to put the major axis vertical, and deprojected to face-on, using as projection parameters $PA = 69^\circ$ and $i = 34^\circ$. The image has then been binned to 256×256 pixels. This R band image covers $8.5' \times 8.5'$ on the sky, corresponding to a radius of 6.24 kpc at the assumed distance of NGC 6946, 5 Mpc. The actual spatial resolution amounts to a few times the cell size, about 200 pc. The following step is to build a good gravitational potential from this image.

As in Garcia-Burillo et al. (1993), the calculation is done in two steps. The axisymmetric part of the potential is obtained by assuming a constant mass to light ratio, and adjusting this constant to reproduce the observed CO and HI rotation curves. The perturbations due to the bar and spiral arms are included in the non axisymmetric part of the potential. The last parameter to adjust is Ω_p , the pattern speed of the density wave (bar + spiral arms). The gas distribution and velocity field are very sensitive to Ω_p . We find that $\Omega_p = 42 \text{ kms}^{-1} \text{ kpc}^{-1}$ gives the best results. The corotation is found at a radius of 3.5 kpc, close to the end of the bar, and the OLR lies outside of the disk. Figure 3a presents the deprojected R-band image. Figures 3b and 3c present an example of the obtained molecular cloud distribution. The gas clouds are concentrated in the spiral arms, with few molecular clouds at radii larger than 4 kpc. The model rotation curve is shown in Fig. 4, together with the angular frequency $\Omega(r)$. We have not attempted to model the compression of diffuse gas in the spiral structure, and have kept an axisymmetric distribution of diffuse atomic gas.

3.3. Stellar population

Once the gas is distributed over the galactic disk, we create OB associations, with star masses ranging from 10 to 60 M_\odot (stellar types from B2 to O5). We have chosen not to include stars less massive than 10 M_\odot because their lifetime becomes a significant fraction of the rotation period. Shortward of 2000 Å, the UV radiation is mostly produced by OB stars and the contribution by late B type stars is at most 20% (Walterbos & Greenawalt 1996, Mathis et al. 1983). The choice of the upper mass cutoff at 60 M_\odot is motivated by the work of Heydari-Malayeri & Beuzit (1994) who have shown that suspected very massive stars ($\sim 100 M_\odot$) are actually clusters of less massive stars. Also, a very short time step is required to sample adequately the lifetime of these very massive stars.

We allow only clouds more massive than $4 \times 10^4 M_\odot$ to form massive stars. In the cells satisfying this criterion, the OB associations are born at the outer edge of the molecular clouds. We have tested different star formation laws, so as to match as well as possible the H α radial profiles. The best fits are obtained with a star formation rate (SFR) depending on the angular frequency and the local gas surface density as proposed by Wyse & Silk (1989) :

$$SFR(\mathbf{r}) = \epsilon \Omega(r) \sigma_{gas}(\mathbf{r})$$

with ϵ the star formation efficiency, $\Omega(r)$ the angular frequency at radius r and $\sigma_{gas}(\mathbf{r})$ the HI+H₂ surface density at position \mathbf{r} in the disk. We find that $\epsilon = 5\%$ provides the best match to the H α radial profile by Kennicutt (1989).

The stellar mass distribution inside an OB association is drawn from the Initial Mass Function (IMF). We have chosen an index close to the Salpeter IMF, as suggested

by measurements in Galactic and extragalactic OB associations (Massey et al. 1995) : $\frac{dN(M)}{dM} = M^{-2.3}$.

The stellar associations are born with a mean velocity relative to their parent cloud chosen from a Gaussian of mean value 10 km s^{-1} and FWHM $\sim 10 \text{ km s}^{-1}$. These figures are in good agreement with observed data by Leisawitz et al. (1989) in their study of the relation of star clusters with molecular clouds. With this value, the average motion of OB stars relative to their parent cloud is 10 pc in 10^6 years. Finally, stars die after a time equal to their Main Sequence lifetimes from Güsten & Mezger (1983). Effective temperatures, stellar luminosities and radii, averaged over the main-sequence lifetime, are taken from Cox et al. (1986). Because we are only interested in broad band fluxes and colors, we have calculated all stellar fluxes, from UV to B bands, in the black-body approximation. Lyman continuum radiation production rates, averaged on the Main Sequence lifetime, are also taken from Cox et al. (1986) and Güsten & Mezger (1983) to have a coherent set of parameters. We use the parametrization as a function of the stellar mass, M :

$$\log_{10}\left(\frac{N_{Lyc}}{s^{-1}}\right) = 38.3 + 8.16 \times \log_{10}(M) - 0.24 \times \log_{10}^2(M) - 0.41 \times \log_{10}^3(M).$$

to compute the thermal radio continuum flux, H α luminosity and Strömgren sphere diameters.

We also include the effects of the radiation of massive stars on neutral gas, and allow molecular clouds to be partially eroded and ionized by the radiation of nearby OB associations, if they overlap with the Strömgren sphere of an OB association. We compute the radius of this sphere, R_{HII} , assuming that all stars are located at the same position and have a global production rate of Lyman continuum photons N_{Lyc} , equal to the sum of the contribution of the individual stars, and for case B recombination in a diffuse medium of density n_H : $R_{HII} = \left(\frac{3}{4} \frac{N_{Lyc}}{\alpha_B n_H^2}\right)^{1/3}$. In this formula, α_B is the hydrogen recombination coefficient (Osterbrock 1989). The mean radius for R_{HII} is 35 pc .

To constrain the population of massive stars, we calculate different stellar outputs, namely we perform a detailed calculation of the UV radiation field at $912\text{--}2000 \text{ \AA}$, and also compute the global U flux and U radial profile, as well as the thermal radio continuum and H α emission.

- 6 cm radio-continuum.

According to Mezger (1972) and Turner & Ho (1994), the radio continuum emission of HII regions for case B recombination, at an electronic temperature T_e of 10^4 K and with 45 % of the ionizing photons being converted into H α photons, is directly related to N_{Lyc} by:

$$\frac{N_{Lyc}}{s^{-1}} = 1.1 \times 10^{50} \left(\frac{S_{6cm}}{mJy}\right) \left(\frac{D}{Mpc}\right)^2.$$

This formula does not include any correction for dust absorption of the ionizing radiation within the HII region.

Current estimations are that nearly 50% of the Lyman continuum may be absorbed by dust.

- H α .

The relationship between the H α luminosity and the production rate of Lyman continuum photons, using the same assumptions as above, can be deduced from Mezger (1972) and Peimbert et al. (1975):

$$\frac{L_{H\alpha}}{L_{\odot}} = 3.55 \times 10^{-46} \left(\frac{N_{Lyc}}{s^{-1}}\right).$$

The correction for the extinction may amount to about 1 magnitude at H α but it is highly uncertain (McKee & Williams 1997, van der Hulst et al. 1988). Because of the uncertainties involved in this correction, we have preferred not to do it. This allows us to check that the energy is conserved with a good accuracy in the simulation.

The formed OB associations have typical production rates of Lyman continuum photons, N_{Lyc} , in the range $10^{45}\text{--}10^{51} \text{ s}^{-1}$. The cumulative Lyman continuum luminosity function of the population is shown in Fig. 5. Its shape is similar to the distribution for Galactic HII regions (McKee & Williams 1997). There is a small excess around $N_{Lyc} \geq 10^{49.5} \text{ s}^{-1}$, dominated by the most massive stars in the younger associations, and a deficiency of associations with $N_{Lyc} \geq 10^{50.5} \text{ s}^{-1}$. As a whole, the match of the two distributions is very good. The distribution of the intrinsic UV luminosity of OB associations extends over four orders of magnitude from 10^4 to $10^7 L_{\odot}$, i.e. from small associations with about 20 stars and a total stellar mass of $600 M_{\odot}$, up to large associations gathering 200 OB stars, including a few 50-60 M_{\odot} stars, and having a total stellar mass of $6000 M_{\odot}$.

3.4. Dust properties

We use the average Galactic extinction curve from Fitzpatrick & Massa (1988) at UV wavelengths. For visible and near infrared wavelengths, we use the work by Seaton (1979). This curve is probably valid on a large scale in the diffuse medium of NGC 6946 which has a similar metallicity to the Milky Way. We assume a constant metallicity and gas to dust ratio in the disk, and use the average value for the Milky Way : $\frac{NH}{E(B-V)} = 5.8 \times 10^{21} \text{ H cm}^{-2} \text{ mag}^{-1}$ and $A_V = 3.1 E_{B-V}$ (Bohlin et al. 1978). The extinction through a cell filled with molecular gas, with the adopted spatial resolution, is 2.5 magnitudes. The dust properties have been summarized by Bruzual et al. (1988) and Witt & Gordon (1996). Apart from the enhanced absorption in the 2175 \AA bump, the dust albedo is fairly constant at UV and visible wavelengths at $\omega \sim 0.55$. We include the coherent scattering of UV light by dust grains. The anisotropy is described using the Henyey-Greenstein (1941) function, where the anisotropy parameter is defined as $g = \langle \cos\theta \rangle$ and θ is the scattering angle.

3.5. Radiative transfer

The observed properties of external galaxies depend on the propagation of the stellar radiation in the interstellar medium. To determine the local radiation field, we follow the propagation of UV photons (912-2000 Å) emitted from the OB stars in the two phases medium. In each cell, we compute a local radiation field. We define the local radiation field in the UV, χ_{UV} , relative to the mean radiation field in the UV at the Solar radius, χ_0 , established by Mathis et al. (1983), so that $\chi_{UV} = \frac{4\pi J}{\chi_0}$. In the Galaxy and at the solar radius, the InterStellar Radiation Field, ISRF in the UV, has been defined as $\chi_0 = 4\pi J = 4\pi \int_{912\text{\AA}}^{2000\text{\AA}} J_\lambda d\lambda = 1.84 \times 10^{-3} \text{ erg cm}^{-2}\text{s}^{-1}$ and through visible/IR bands as $G_0 = 4\pi \int_{912\text{\AA}}^{2\mu\text{m}} J_\lambda d\lambda = 2 \times 10^{-2} \text{ erg cm}^{-2}\text{s}^{-1}$, where J_λ is the specific intensity of the radiation field averaged over 4π sr (Mathis et al. 1983).

On their path, photons can be scattered and/or absorbed by dust in both neutral phases. We have chosen not to follow individual photons which would have been time consuming, but to use instead pseudo-photons representing a collection of N photons. We are then able to probe a larger area with a lower number of photons. We sample the 912-2000 Å interval with 20 bins of constant wavelength width $\Delta\lambda$, and launch n_γ pseudo-photons per association per wavelength bin. The longward limit has been set to 2000 Å, to avoid having to take into account the contribution from star types later than B to the ISRF (Walterbos & Greenawalt, 1996).

The pseudo-photons emitted by the OB association number i carry a fraction $f_\lambda^i d\lambda$ of the luminosity L_λ^i radiated by this OB association. They travel from the center of a cell (size r_{cell}) to an adjacent one, and the energy absorbed by the interstellar medium, when non-zero, is left on the common face of these 2 cells. The absorbed energy is reprocessed in the far-infrared. The pseudo-photon energy along its path from association number i can be written as :

$$f_\lambda^i d\lambda = \alpha^i \frac{L_\lambda^i}{n_\gamma}$$

In this formula, $\alpha^i = \prod_j \alpha^j(x, y, z)$ is the product of the probabilities for non absorption in each cell along the travel from the OB association number i to the cell position (x, y, z) , or with $\omega(\lambda)$ the dust albedo and τ_λ the total cell opacity including scattering :

$$\alpha^j = e^{-(1-\omega(\lambda))\tau_\lambda}$$

in the diffuse phase, and

$$\alpha^j = \omega(\lambda)$$

in the H₂ phase.

When leaving an OB association, the direction for each pseudo-photon is uniformly chosen on the unit sphere. These pseudo-photons travel in the two-phase interstellar medium. There are different possibilities when reaching a new cell :

- i) The gas in the cell is diffuse and atomic. Then the pseudo-photon can either :
 - be absorbed partially in the cell. A fraction of the luminosity is left, and the pseudo-photon continues in the same direction with a lower luminosity.
 - be scattered.

- ii) The cell is filled with molecular gas.

The pseudo-photon is partly absorbed, and partly backward scattered, the ratio between the energy left in the cell and the total energy of the pseudo-photon depends on the albedo as $1 - \omega(\lambda)$. We have chosen backward scattering in that case to prevent the pseudo-photon from interacting with the same molecular cloud several times.

After a scattering event, a scattering angle θ is chosen according to the anisotropy function, and the azimuthal angle ϕ is uniformly chosen in the interval $[-\pi, \pi]$. Then the new direction is easily deduced from the previous one (Witt 1977).

Since we cannot store all the pseudo-photons' incident directions, and in order to define an isotropic radiation field in each cell, we assume that the equivalent surface of the cell is $6r_{cell}^2$. Then, the UV radiation field in the cell (x, y, z) due to the contributions of all pseudo-photons travelling through this cell, can be expressed relative to the Galactic ISRF χ_0 as :

$$\frac{\chi(x, y, z)}{\chi_0} = \sum_i \sum_{\delta\lambda} \frac{f_\lambda^i d\lambda}{\chi_0 6r_{cell}^2}$$

Because of the coarse angular resolution and the low number of pseudo-photons leaving each OB association, the resultant map of the radiation field presents strong fluctuations. We have chosen to smooth the map of the radiation field by averaging the data in nearby cells, typically 3x3 cells. Furthermore, some cells are never visited by UV photons, for example in the interarm region or in the outer disk ($r \geq 5$ kpc). In that case, we use as incident radiation field, the Galactic ISRF (longward of 2000 Å), scaled by the local surface brightness in the R band image to take into account the radial variation of the radiation field from the old stellar population between the central regions ($r \leq 1$ kpc) and the outer disk ($r \geq 5$ kpc). The reference value is given in units of $4\pi \int_{2000\text{\AA}}^{2\mu\text{m}} J_\lambda d\lambda = G_0 - \chi_0 = 1.82 \times 10^{-2} \text{ erg cm}^{-2}\text{s}^{-1}$. The position for the reference value has been chosen at the edge of a spiral arm, at a distance $r = 4$ kpc from the center, where the UV radiation field χ_{UV} is close to 1.

3.6. Emergent emission.

Once the local UV energy density has been calculated, models are used to determine the C⁺ and FIR emissions from each cell, assuming that they arise from the same area as the one used for the calculation of the UV radiation field. For the dust emission, we use the model by Désert et al. (1990), which has 3 different components: PAHs which

are fully ionized when $\chi_{UV} > 1$, very small grains and big grains. We calculate the dust emission in the four IRAS bands at 12, 25, 60 and 100 μm plus an additional band at 200 μm , as the reprocessing of the combination of the UV radiation field (912 - 2000 Å) described by χ_{UV} and of the ISRF for the 2000 Å-2 μm part of the spectrum. We decrease the PAH abundance in large radiation field environments, as suggested by Ryter et al. (1987), to one fifth of the standard value when $\chi_{UV} > 100$.

Very large molecular clouds, with masses larger than $10^6 M_\odot$ occupy more than 4 cells in the grid. The inner cell is not directly exposed to the UV radiation and for this cell we assume that the ISRF is attenuated by 2.5 magnitudes of visual extinction.

We assume low optical depth in the mid and far infrared. From the analysis of the COBE maps of the Galaxy, Boulanger et al. (1996) deduce $\tau_\lambda/N_H = 1 \times 10^{-25} \text{ cm}^2 \text{ H}^{-1} (\lambda / 250 \mu\text{m})^{-2}$, which combined with the mean column density of individual clouds, $N_H = 1.5 \times 10^{22} \text{ cm}^{-2}$, gives an opacity of 2×10^{-3} at 200 μm .

According to the dominant phase in a given cell of the model, the emergent infrared emission can be :

- reprocessing of the whole incident stellar radiation for molecular clouds which are totally optically thick in the UV. All impinging radiation is completely reprocessed in infrared emission from the outer cells of molecular clouds,
- proportional to the gas column density for the diffuse medium, which is optically thin in the UV. We assume no UV extinction at the 12 pc scale.

We use the PhotoDissociation Region (PDR) model by Le Bourlot et al. (1993) to estimate the $^2P_{3/2} - ^2P_{1/2}$ C⁺ emission at the surfaces of molecular clouds. We use a constant molecular hydrogen density of $5 \times 10^3 \text{ H}_2 \text{ cm}^{-3}$ and the incident UV field χ_{UV} . The density is not a critical parameter as long as it is higher than the critical density for collisional excitation of C⁺ (1000 H cm^{-3}) (see Tielens & Hollenbach 1985). Furthermore, we assume that the whole surface of clouds contributes to the C⁺ emission. As for the C⁺ emission from the diffuse neutral phase, we use the model by Wolfire et al. (1995) for a two phase neutral atomic medium. Finally, the contribution from the ionized gas in the HII regions around the OB associations is also included. We assume that the gas has the same density as the diffuse medium, $n_e = n_H$ and an electronic temperature of 10^4 K . The total C⁺ luminosity from an HII region of radius R_0 is then proportional to the volume of the HII region with a correction factor to take into account the other ionization stages of carbon.

Because we deal with a line, the opacity may not be small depending on the gas distribution and viewing geometry. In fact, opacity effects are important at large inclination angles. To obtain an edge-on view of the model galaxy in the $^2P_{3/2} - ^2P_{1/2}$ C⁺ line, we have made an accurate calculation of the radiative transfer in this line. For each line of sight through the disk, we sample the line profile with bins of 1 kms^{-1} width, and calculate the emergent

intensity in each velocity bin, including saturation effects. We assume that the intrinsic velocity dispersion of a PDR is 1 kms^{-1} . For the diffuse medium, the velocity dispersion is 10 kms^{-1} . We do not account for absorption in the far infrared continuum. We obtain $\tau_{C^+} = 0.40$ for an edge-on view, and $\tau_{C^+} = 0.10$ for a face-on view.

3.7. Implementation of the model

To avoid transient stages of the simulation, the code is evolved during a few time steps. We stop the simulation when stable results are obtained on a time scale of 20 Myrs. This time scale corresponds to about half the lifetime of a giant molecular cloud before disruption by photoevaporation. This is the reason why we can not integrate further in time without treating gas recycling. The time step has been fixed at 10^6 years, shorter than the lifetime of the most massive stars. We have checked the reliability of the calculations by different tests:

- We have verified that the total UV luminosity from the stellar population emerges from the galaxy either at the same wavelength, or at far infrared wavelengths for the light reprocessed by dust grains. The total luminosity is conserved with an accuracy of 1 %.
- When the number of pseudo-photons leaving each OB association n_γ is too small, the map of UV radiation field is noisy with a few extremely bright spots and large voids. This is due to undersampling of the galaxy volume. The number of pseudo-photons should be as large as possible, but we have verified that we obtain a good map of the UV radiation field with 100 pseudo-photons per OB association. The map is smooth in the vicinity of the OB associations, hence the ratio of FIR emissions from the diffuse and dense gas stays constant with increasing n_γ .
- The cell size is also a critical parameter: since χ_{UV} is proportional to r_{cell}^{-2} , it might be underestimated for small clouds very close to OB associations. This has severe consequences for the C⁺ emission, which scales roughly as $r_{cell}^2 \log(\chi_{UV})$, but little or none for the FIR emission which varies as $r_{cell}^2 \chi_{UV}$ since in that case there is no resultant scaling with r_{cell} . To test the validity of the adopted resolution, we have performed a run restricted to one quadrant only, with a cell size of 6.1 pc. We observed no large variation in the C⁺ emission and thus conclude that the adopted resolution of 12 pc is correct for our purpose. Note that the volume filling factor decreases to 1.3 % in the high resolution run, because we fill the space in a more accurate way using a higher spatial resolution.

4. Results

Table 2 summarizes the input parameters for the Standard Model, and Table 3 presents the results. The star formation rate from 2 to 60 M_\odot is fixed at $4.0 M_\odot \text{ yr}^{-1}$, with a star formation efficiency ϵ of 5%, as defined in Sect. 3.4. With these values, the modelled H α luminosity and

H α radial profile are in quite good agreement with the observed data (Kennicutt 1989). This is also true for the UV luminosity at 2000 Å and the 6 cm luminosity. We are thus confident that the massive star population is well constrained by the observed data. With a low mass cut-off at 10 M $_{\odot}$ stars, we overestimate the UV luminosity at 2000 Å of the modelled stellar population by 20%, because we miss the contribution to the UV continuum of lower mass stars, between 2 and 10 M $_{\odot}$.

4.1. Disk opacity in the UV

We have computed an average opacity over the galaxy in the UV and for the H α line. We define this opacity as : $\tau = -\ln(L^{\text{emergent}}/L^{\text{emitted}})$ where L^{emitted} is the total luminosity in the disk at a given wavelength and L^{emergent} is the emergent luminosity. This opacity is computed for two different viewing angles of the model, $i = 0^\circ$ for face-on and $i = 90^\circ$ for edge-on. We have found a significant opacity for the face-on view, at 1000 Å, 2000 Å and for H α , namely $\tau(1000\text{Å}) = 0.8$, $\tau(2000\text{Å}) = 0.7$, $\tau(H\alpha) = 0.60$ for the whole galaxy.

The opacity is controlled simultaneously by the geometry of the molecular cloud ensemble and by the diffuse medium. If we ignore the extinction due to the diffuse component, we find an opacity of 0.51 at 1000 Å. This value is due to geometrical effects, mostly blocking of the UV radiation by molecular clouds, and it does not depend on wavelength. Thus we can write the opacity at any wavelength in the UV as $\tau_\lambda = 0.51 + \tau_\lambda^{\text{HI}}$, the second term accounting for the wavelength dependence of the extinction in the diffuse medium.

A global opacity of $\tau \simeq 0.8$ corresponds to a fraction of approximatively 45% of the far UV stellar radiation leaving the galaxy disk, mostly above or below the main plane. Most of these photons have not been scattered because the probability of leaving the disc after a scattering event is low. This significant fraction of the radiation from massive stars leaking out of HII regions could contribute to the maintenance of the Reynolds layer of ionized gas. The derived face-on opacity at 2000 Å, 0.7, falls well within the range of opacities derived by Buat & Xu (1996). The mean extinction in their sample of nearby spiral galaxies is $\simeq 0.9$ mag at 2000 Å. Though the opacity is not very large, the mean distance travelled by a UV photon before absorption is quite small, 440 pc, roughly equal to the HI disc thickness. As shown on Fig. 6, there are however photons travelling to much larger distances, 1 to 2 kpc, with a small probability (0.01). Conversely, many zones in the interarm receive very few UV photons. Due to the lower gas density, few OB associations are created in the interarm region. The numerous OB associations in the arms are too distant to contribute to the local radiation field since the arm/interarm separation is larger than 1 kpc in the disk.

The distribution of χ_{UV} values provide further information on the radiation field resulting from the OB associations (Fig. 7). Whereas most of the galaxy is exposed to a low UV radiation field, it is possible to find regions with high UV intensity ($\chi_{UV} \geq 1000$) even at a moderate spatial resolution. The total dynamical range of the UV radiation field extends over more than 4 orders of magnitude. This huge variation can be explained by the close association of OB associations and molecular clouds: in a galaxy with a prominent spiral structure, OB associations are born in the spiral arms, where the gas density is the highest. This maximizes both the illumination of molecular clouds by UV radiation and the absorption of UV radiation by molecular gas, hence the heating of molecular gas. For the model galaxy, we find that 30 % of the total number of cells with molecular gas are exposed to a strong or median radiation field ($\chi_{UV} \geq 10$). These cells are located in 40% of the molecular clouds. This figure is comparable to the clouds in Milky Way: Solomon et al. (1985) found that in the Galaxy, at a resolution greater than 10 pc, 25 % of the molecular clouds are warm and associated with HII regions. Also, Williams and McKee (1997) estimate that at least one OB star is present in half of the giant molecular clouds with masses larger than 10^5 M $_{\odot}$. The probability to find massive stars or clusters associated with a giant molecular cloud increases sharply with the cloud mass and reaches almost 1 for masses larger than 8×10^5 M $_{\odot}$ (Williams & MacKee 1997). Our numerical results are in agreement with these facts.

4.2. Far infrared emission

We now discuss the emergent radiation from the model galaxy and start with the infrared emission. As in the Désert et al. (1990) dust model, the luminosities in the IRAS bands are computed as $4\pi D^2 \nu S_\nu$, where S_ν is the total observed flux density and D is the distance to the object. The infrared colors are given as the flux density ratios, to compare with observed data.

The model galaxy has very similar emissions as NGC 6946 at 60-100 & 200 μm , with outputs of 5.1, 8.5 and 4.9×10^9 L $_{\odot}$, corresponding to 114%, 128% and 144% of the luminosities observed at those wavelengths. The far infrared emission comes from both the molecular and atomic gas phases.

The UV radiation is the main heating mechanism of the dense and diffuse gas phases, with contributions of 4.2×10^9 L $_{\odot}$ and 6.1×10^9 L $_{\odot}$ at 60 & 100 μm . The contribution to the FIR emission of the old stellar population, described by the ISRF, is a factor 3 lower, with 0.9×10^9 L $_{\odot}$ and 2.4×10^9 L $_{\odot}$ in the 60 & 100 μm bands. The situation is different at 200 μm , where dust grains heated by the UV radiation or by the ISRF have almost equal contributions to the total luminosity: 3.0×10^9 L $_{\odot}$ for the UV and 1.9×10^9 L $_{\odot}$ for the ISRF. The contribution from the inner parts of clouds illuminated by the attenuated ISRF

is only $0.5 \times 10^8 L_{\odot}$. As a whole, 72 % of the far infrared luminosity can be attributed to UV heated gas, which is mostly molecular. The remaining 28% corresponds to dust heated by the ISRF, at locations far away from the OB associations.

The diffuse and dense phases have similar contributions to the total FIR emission, with a slight excess from the molecular clouds, 54 % versus 46 % from the diffuse gas. This significant contribution from the diffuse gas is due to the fact that it occupies a large fraction of the galaxy volume. Hippelein et al. (1996) also conclude from ISO observations of other nearby galaxies (M51, M101) that the neutral atomic gas has an important contribution to the far infrared emission. The contribution from the atomic gas may be underestimated because we do not take into account the compression of the diffuse gas in the spiral structure. Comparing with molecular clouds, we can estimate that, having atomic gas concentrated in the spiral arms would result in a brighter FIR emission, with a slightly warmer color temperature since the dust grains would be closer (in average) to the heating sources. A precise estimate of the magnitude of the effect is beyond the scope of this paper.

The global infrared excess for the model galaxy, IRE, is defined as the luminosity ratio $IRE = L_{12-100\mu m} / L_{Ly}$, with $L_{Ly} = N_{Ly} h\nu_{Ly}$ and $h\nu_{Ly} = 13.6$ eV. At the disk scale, the IRE takes the value 5.9, in agreement with observations of Galactic HII regions (Caux et al. 1985, Myers et al. 1986).

The diffuse and dense gas (atomic and molecular) have the following contributions to the total luminosity of the C⁺ 158 μm line: 77% from the dense phase and 23% from the diffuse phase. Less than $10^4 L_{\odot}$ comes from HII regions. The total emission of the galaxy is $2.5 \times 10^7 L_{\odot}$, a factor 2.5 lower than the measured value, $6.3 \times 10^7 L_{\odot}$ (Madden et al. 1993). Compared to the 60-100 μm far infrared emission, the C⁺ line represents 0.21% of the FIR (60-100 μm) emission. This figure is comparable to the observed ratio for other spiral galaxies with 0.1 - 1 % (Lord et al. 1996). Nevertheless, the value for NGC 6946 was found to be 0.6 % (Madden et al. 1993), and in the Galaxy, Shibai et al. (1991) and Wright et al. (1991) have measured $L_{C^+} = 0.7 \% L_{FIR}$ with the same definition of L_{FIR} as above.

4.3. Radial profiles

The 60 μm radial profile is shown on Fig. 8a. There is a large decrease from the inner to the outer parts of the disk, about two orders of magnitude. In NGC 6946, the same behaviour has been observed by Tuffs et al. (1996) using ISO. Averaged over the model, the S_{60}/S_{100} infrared color appears to be slightly different in the two phases: 0.32 for the diffuse phase and 0.38 for the dense phase. This FIR color decreases with increasing radius from 0.40 in

the center to 0.23 at $R \simeq 5$ kpc (Fig 8b), in agreement with the maps by Engargiola (1991). The decrease is seen in both phases, with S_{60}/S_{100} ranging from 0.35 to 0.23 for the diffuse phase, and from 0.42 to 0.28 for the dense phase.

The radial profile of the intensity of the C⁺ $^2P_{3/2} - ^2P_{1/2}$ 158 μm line (Fig. 8c) shows a much flatter gradient than the FIR emission. This is due to the logarithmic dependence of the line intensity on the incident radiation field in PDRs. As shown in Fig. 8c and 8d, the diffuse atomic gas is the main source of C⁺ emission at large distance from the nucleus, for radii larger than 4 kpc. It is thus possible to determine the intrinsic L_{C^+}/L_{FIR} luminosity ratio from the two gas phases, using the data at $R \sim 2$ kpc for the molecular gas and data at $R \geq 5$ kpc for the atomic gas. We find that L_{C^+}/L_{FIR} is equal to 0.10 % in the diffuse phase and to 0.25% in the dense phase.

4.4. Maps

We show on Fig. 9 face-on maps of 100 μm , C⁺ and UV(912-2000 Å) emissions. Edge-on maps at the same wavelengths are shown in Fig. 10 for comparison. Compared to the C⁺ observations of the edge-on galaxy NGC 891 (Madden et al. 1994), there is an overall agreement. In particular, the scale height in C⁺ is predicted to be larger than the scale height of the CO emission, due to the contribution of the diffuse neutral and ionized media which have a larger scale height (Fig. 11).

In the face-on C⁺ map, there is a large hole in the inter-arm regions in the NW, at a similar position to the hole detected by Madden et al. (1993) with the KAO. This hole is due to the lower density of molecular gas and of OB associations in the interarm regions. Therefore few UV photons illuminate this region and the radiation field is very low. The map shows many details and a large contrast between arm and interarm regions. We have smoothed the image from the model to the resolution of the KAO observations (50'' beam = 1.2 kpc at the distance of NGC 6946). The contrast between the brightest regions and the disk drops by a large factor. This resolution effect may explain the low dynamical range found in the observed data. If PDRs are the main source of C⁺ 158 μm radiation in galaxies, we predict that the emission should have more contrast at higher spatial resolution. This could be tested by maps of external galaxies made with the future Stratospheric Observatory For Infrared Astronomy (SOFIA).

The edge-on maps at 100 μm and in C⁺ are fairly symmetrical with respect to the center. The edge-on C⁺ map shows however a hole in the central region ($r < 500$ pc) which does not appear on the 100 μm map. This hole is largely due to the large opacity for these lines of sight ($\tau_{C^+} = 0.4$).

4.5. Sensitivity of the model to input parameters

The model results are of course sensitive to the input parameters, therefore we have run different models deviating from the standard model by one parameter.

Because of the poor knowledge of the albedo in UV, we have run a model with a lower albedo of dust grains, $\omega = 0.4$. We find that the opacity increases to 1.0 at 1000 Å & 0.90 at 2000 Å. The 60 μm emission from the dense phase increases by 5%, while the 100 and 200 μm emissions both decrease by 10%. This difference in far infrared emission is due to the moderate increase of the opacity which leads to a warmer dust temperature. The effect on the emission from the diffuse phase is negligible.

A more extreme case is for a null albedo, suppressing any scattering effect. In that case, we maximize the UV opacity and the FIR emission. The opacity increases to 1.25 at 1000 Å and 1.01 at 2000 Å respectively. As a result of this larger absorption, the 60-200 μm emission increases by 47 % as compared to the standard model.

In another run, we have kept the total mass of molecular gas constant, but used a lower mean density, 20 $\text{H}_2 \text{ cm}^{-3}$ instead of 50 $\text{H}_2 \text{ cm}^{-3}$, to increase the clouds sizes. The volume filling factor is then 3.8 %. These larger clouds block more light, and 30 % only of the molecular cells are heated, instead of 40% in the standard model. As a result, the 60-200 μm luminosity decreases by 10%, to $16.7 \times 10^9 L_\odot$.

We have also investigated the effect of the number of OB associations: we have kept the same star formation rate but have gathered adjacent associations to form more powerful sources. As a consequence, n_{OB} decreases from 12000 to 3000. Then a smaller fraction of the cloud population is heated, 15%, as compared to 40% in the standard model. But because these cells are heated by more powerful OB associations, the far-infrared emission is larger and reaches $20.4 \times 10^9 L_\odot$. Thus the FIR emission depends slightly on the number of associations. The C⁺ emission decreases to $1.8 \times 10^7 L_\odot$, because of the smaller number of illuminated clouds.

If we now increase the SF efficiency, from 5 to 10%, so as to double the UV luminosity, the production rate of Lyman continuum photons increases by 80 %. In that case, the mean UV opacity is 0.78. The FIR 60-200 μm luminosity increases by 55 % to $28.7 \times 10^9 L_\odot$. This shows that the FIR emission is not a linear function of the UV luminosity in our model. This non-linear behaviour arises because the opacity is largely controlled by geometrical effects. With a larger star formation activity, HII regions are very large and can destroy molecular clouds efficiently. Thus the mass of molecular gas decreases in the model with a higher SFR. This is the main reason for the non-linear behaviour. This result has been established with the same number of OB associations, while an increased SFR will probably lead to more associations in the disk. How-

ever we have previously shown that the FIR emission does not depend strongly on the number of OB associations.

We have investigated the effect of the atomic density on the size of HII regions, because we probably overestimate the diameter of HII regions, using a mean atomic density and neglecting the dust absorption. If the local gas density is multiplied by two, the volume of the Strömgren sphere is 4 times smaller than in the standard model. The 60-200 μm luminosity of dense molecular gas increases by 10% to $1.1 \times 10^{10} L_\odot$. This is explained by the reduced destructive effect of HII regions on molecular clouds, and then the larger chance for photons to be absorbed by molecular gas. The respective contributions from the diffuse and dense gas to the FIR(60-200 μm) are now 34% and 66%.

This last test shows that the distance between clouds and OB associations has a strong influence on the UV re-processing by dense gas. For the standard model, we have calculated the mean distance between an OB association and the nearest cloud edge, $d_{OB/cloud}$, and have found a value of 35 pc, the mean distance between clouds centers is 37 pc. To have a larger separation between clouds and OB associations, we have increased v_{escape} to 30 kms^{-1} . We obtain $d_{OB/cloud} = 39$ pc. The FIR(60-200 μm) emission from the dense phase decreases by 15% because of the smaller solid angles of the clouds viewed from the associations. As for the FIR (60-200 μm) from the diffuse phase, it slightly increases by 6%.

We have shown that part of the UV opacity is due to geometrical effects. Indeed the UV opacity is lower when the molecular clouds are distributed uniformly in the disk. We have used an earlier epoch of the simulation, when the distribution of gas clouds is axisymmetric. We have kept the same value for the other parameters (number of OB associations, star formation rate, etc.). In that case, the clouds occupy a larger fraction volume of the galactic disk, and the mean distance between clouds increases. Because of this larger mean distance between clouds, the opacity at 1000 Å decreases to 0.47.

5. Discussion & conclusions

We have shown that with simple assumptions about the birth of massive stars and their relationships with the ISM, we can reproduce qualitatively and quantitatively the characteristics of the UV, H α and FIR emissions of a particular object, the Sc galaxy NGC 6946. For such a galaxy with a prominent spiral structure, having a large mass of neutral gas, and forming stars actively, the observed far infrared emission is produced both in molecular gas and in the diffuse atomic gas. More precisely, 54 % of the FIR (60-200 μm) emission comes from dust grains in giant molecular clouds. Dust in the diffuse neutral atomic gas contributes to about 46 % of the total FIR luminosity.

We have evaluated the respective contributions of the UV radiation from massive stars and of the radiation field

from the old stellar population. We find that 72 % of the FIR luminosity can be attributed to UV heated dust grains, which reside mostly in molecular clouds envelopes. The remaining 28 % is due to dust heated by the radiation field from the old stellar population at locations far away from OB associations.

We have calculated the emission of the model galaxy in the $^2P_{3/2} - ^2P_{1/2}$ fine structure line of C⁺ at 158 μm . In the spiral arms, photon dissociation regions at the surfaces of molecular clouds are the main source of the emission. We have found a large arm-interarm contrast in this line. This effect could be tested by high angular resolution maps of galaxies. It results naturally from the combination of a lower gas density and lower radiation field in the interarm regions, because of the short mean free path for UV photons, ~ 440 pc. As a whole, PDRs represent 76% of the emission. The contribution from the diffuse phase is found to be ~ 24 %. Our model is able to account for about 40 % of the observed C⁺ emission of NGC 6946. The emission from PDRs should be viewed as a lower limit since we use the model by Le Bourlot et al. (1993) with low abundances of carbon and other elements in the gas phase: $[\text{C}]/[\text{H}] = 3 \times 10^{-5}$. The average value is 1.3×10^{-4} for Galactic diffuse clouds (Snow & Witt 1996), a factor of 4 larger than the value used in the model. Since the C⁺ 158 μm emission scales roughly with the column density, hence the carbon abundance, the total C⁺ luminosity from PDRs could be larger by at least a factor three than our current model prediction. This would increase the contribution from PDRs to the total C⁺ emission of the model galaxy: with this scaling factor, the predicted C⁺ luminosity of PDRs would reach $6 \times 10^7 L_{\odot}$. Moreover, the C⁺ emission from the diffuse gas is overestimated, because the model of Wolfire et al. (1995) assumes $[\text{C}]/[\text{H}] \sim 3 \times 10^{-4}$ in the gas. Thus the diffuse emission could be 2-3 times smaller than in our standard model. Adopting $[\text{C}]/[\text{H}] = 1.3 \times 10^{-4}$ in both phases would thus enhance the differences of $L_{\text{C}^+}/L_{\text{FIR}}$ between dense and diffuse gas.

The knowledge of the cloudy nature of the ISM, and of the global structure of the galaxy, is important to determine how far UV photons can travel away from OB associations. The filling factor and the mass/radius scaling law appear to be major parameters for the transfer of stellar radiation in the galaxy disk, because they determine at the same time the obscuration and the size of the emitting regions. Other important parameters are the number of OB associations and the sizes of HII regions, because with a large number of OB associations or with small HII regions, molecular clouds are on average closer to massive stars, and are thus more efficiently heated.

In all the models we ran, we have found that the average internal UV opacity is of the order 0.8. The discs are therefore moderately opaque in the UV, as measured by Buat & Xu (1996). This moderate opacity holds for face-on discs. Edge-on discs are quite opaque, with a small fraction of the luminosity escaping, less than 1.0% of the

face-on luminosity. This fraction corresponds to an equivalent extinction of 5 magnitudes in the UV.

These results have been obtained using a crude description of the interstellar medium. The adopted spatial resolution results from a compromise between astrophysical requirements and computational needs, but is certainly very poor compared to the complexity of the interstellar medium. The good agreement of the observed and predicted large scale properties shows nevertheless that the transfer of UV radiation, and the role of the radiation for the gas and dust heating, are correctly described at the 12 pc scale. This is in agreement with previous works estimating that dust heating by UV radiation occurs principally at large distances from massive stars (Murthy et al. 1992, Leisawitz & Hauser 1988).

Acknowledgements. We have benefited from the help of F. Viallefond for the numerical calculations and the data processing, and from discussions with D. Beck, G. Helou, S. Madden, S. Shore. We thank F.X. Désert and J. Le Bourlot for letting us use their codes, and M.G. Wolfire for providing unpublished results.

—

Figure captions

Fig. 1. CO(J=2-1) map at 13'' resolution obtained with the IRAM 30m radiotelescope.

Fig. 2. V-I image, obtained with the 1.20m telescope at the Observatoire de Haute Provence (P. Boissé, private communication). The field of view is 10' by 10', the pixel size is 2.3''. The gray scale runs from white for blue colors to black for red colors.

Fig. 3a. R band image of NGC 6946 used as input for the calculation of the gravitational potential. Field stars have been removed, the image has then been rotated and de-projected to get a face-on view of NGC 6946.

Fig. 3b. A face-on view of the model galaxy, with molecular clouds drawn as circles and OB associations drawn as stars. Only 20 % of the OB associations and molecular clouds are drawn.

Fig. 3c. A close-up view of Fig. 3b. The clouds are drawn at their exact size in the model.

Fig. 4. Adopted rotation curve (dot-dashed line), angular frequency $\Omega(r)$ (full line), and $\Omega \pm \frac{\kappa}{2}$ curves. The corotation for the adopted pattern speed is located at $r = 3.5$ kpc.

Fig. 5. Distribution of the production rate of Lyman continuum photons N_{Lyc} , for the modelled population of OB associations (full line) in NGC 6946, and for the Galaxy (dot-dashed curve) (McKee & Williams (1997)). The plot can be read for instance as 500 OB associations out of 12000 have $N_{Lyc} > 10^{50} \text{ s}^{-1}$.

Fig. 6. Distribution of the distance from their parent OB association, travelled by UV photons before absorption. The median distance is 120 pc, and the mean distance is 440 pc.

Fig. 7. Distribution of the UV intensity measured relative to the ISRF in the modelled galaxy, for cells filled with diffuse gas (dot-dashed line) and for cells filled with molecular gas (full line).

Fig. 8a. Radial profiles of the 60 μm surface brightness. The thin solid line shows the combination of the two gas phases, while the triangles show the contribution of the diffuse atomic gas, and the squares the contribution from the molecular gas. The thick solid line shows the mean radial profile deduced by Engargiola (1991) from an IRAS image.

Fig. 8b. Radial profiles for the ratio of 60 and 100 μm fluxes, global and for the two phases.

Fig. 8c. Radial profiles of the C⁺ emission: global and for the two phases.

Fig. 8d. Radial profiles of $L_C^+ / L_{(60-100\mu\text{m})}$: global and for the two phases.

Fig. 9. Face-on views of:

a) 100 μm emission, at 48 pc resolution. The gray scale ranges from 1 to $10^3 \text{ L}_\odot \text{ pc}^{-2}$. We have overlaid contours of the same map convolved with a 750 pc beam: the levels are at 10, 30, 60, 100, 200 $\text{L}_\odot \text{ pc}^{-2}$.

b) C⁺ line, at 48 pc resolution. The gray scale ranges from

10^{-2} to $1 \text{ L}_\odot \text{ pc}^{-2}$. Overlaid contour levels from 0.1 to 0.6 by $0.1 \text{ L}_\odot \text{ pc}^{-2}$ for the same image convolved with a 750 pc beam.

c) emergent UV surface brightness (resolution: 48 pc). The gray scale ranges from 10^{-2} to $10^5 \text{ L}_\odot \text{ pc}^{-2}$.

Fig. 10. Edge-on views of NGC 6946, at 48 pc resolution. The linear scale is not identical for both axes.

a) 100 μm IRAS band, with contour levels at 10^3 , 3×10^3 , 6×10^3 and $10^4 \text{ L}_\odot \text{ pc}^{-2}$.

b) C⁺, at the same resolution, accounting for the line opacity. The gray scale ranges from 0 to $50 \text{ L}_\odot \text{ pc}^{-2}$. Contour levels from 10 to 50 by $10 \text{ L}_\odot \text{ pc}^{-2}$.

Fig. 11. Average vertical profiles through the disk for the C⁺ (dot-dashed line) and CO(1-0)(full line) emissions. The CO(1-0) profile presents a smaller scaleheight (40 pc) than the C⁺ profile (100 pc). We have assumed that the CO(1-0) emission is proportional to the molecular gas column density.

Table 1. Observed parameters for NGC 6946.

Observed data	Value	Reference
Distance	5 Mpc	De Vaucouleurs (1979)
Inclination	34°	Considère & Athanassoula (1988)
M _{H2} (R < 6')	2.0 10 ⁹ M _⊙ ¹	Young & Scoville (1982)
M _{HI} (R < 6')	2.6 10 ⁹ M _⊙ ²	Boulanger & Viallefond (1992)
L _{1950–2050Å}	5.4 10 ⁸ L _⊙ ³	Buat et al. (1989)
L _{Hα}	1.0 10 ⁸ L _⊙ ⁴	DeGioia et al. (1984))
B _t ⁰	8.49 mag	RC3
IRAS 12μm	2.3 10 ⁹ L _⊙ ± 20 % ⁵	Engargiola (1991)
IRAS 25μm	1.4 10 ⁹ L _⊙ ± 20 % ⁵	Engargiola (1991)
IRAS 60μm	4.5 10 ⁹ L _⊙ ± 20 % ⁵	Engargiola (1991)
IRAS 100μm	6.6 10 ⁹ L _⊙ ± 20 % ⁵	Engargiola (1991)
IRAS 200μm	3.4 10 ⁹ L _⊙ ± 20 % ⁵	Engargiola (1991)
L _{C+}	6.3 10 ⁷ L _⊙ ⁶	Madden et al. (1993)
S _{6cm} ^{thermal}	83 mJy ± 25 % ⁷	Klein et al. (1982)

We use the value 3.8×10^{33} erg s⁻¹ for the solar luminosity at any wavelength.

¹ We use $N_{H_2}/I_{CO(1-0)} = 2.3 \times 10^{20}$ mol cm⁻²/(K kms⁻¹) and a total intensity $I_{CO(1-0)} = 569$ Kkms⁻¹ in a 45" beam, we do not account for projection effects.

² We use $M_{HI} = 1.9 \times 10^{10}$ M_⊙ at a distance of 10 Mpc, corresponding to 4.7×10^9 M_⊙ for a distance of 5 Mpc. By performing an integration over the HI map, we estimate that the part with R < 6' contributes to 55 % of the global emission.

³ The 2000 Å flux, 6.92×10^{-12} erg cm⁻²s⁻¹Å⁻¹, is corrected for the Galactic extinction and integrated over a 100 Å band. Note that Donas & Deharveng (1987) have reported a flux at 2000 Å twenty times lower (1.66×10^{-13} erg cm⁻²s⁻¹Å⁻¹). Measurements at other UV wavelengths are available in Rifatto et al. (1995).

⁴ We use the uncorrected flux $f_{H\alpha} = 1.31 \times 10^{-10}$ erg cm⁻²s⁻¹ and the relationship $L_{H\alpha} = 3.13 \times 10^{16}$ D_{Mpc}² $f_{H\alpha}$ from Young et al. (1996). We have subtracted the contribution from the nucleus, estimated to be 20 % of the total luminosity. Note that Young et al. (1996) give a lower total flux, 3.38×10^{-11} erg cm⁻²s⁻¹, while Kennicutt (1989) reports a mean surface brightness of 4.2×10^{32} erg s⁻¹ pc⁻² corresponding to a total Hα luminosity of 3×10^7 L_⊙ at the adopted distance.

⁵ We estimate the luminosity in the band centered on frequency ν , by νF_ν . We use the IRAS and KAO fluxes reported by Engargiola (1991) for a radius R < 5.6' and correct from the contribution of the nucleus (central 45") to obtain 12 Jy at 12μm, 15 Jy at 25μm, 114 Jy at 60μm, 283 Jy at 100μm and 288 Jy at 200μm. The global color for the disk is $S_{60}/S_{100} = 0.40$. The far infrared luminosity is $L_{FIR(60-100\mu m)} = L_{60\mu} + L_{100\mu} = 1.1 \times 10^{10}$ L_⊙, $L_{FIR(60-200\mu m)} = 1.45 \times 10^{10}$ L_⊙.

⁶ We have excluded the contribution of the nucleus and rescaled the data by Madden et al. (1993) for the adopted distance.

⁷ We use an estimation of 625 mJy for the total flux at 6cm (Klein et al. 1982), subtract the nuclear contribution estimated to be 33% of the total flux, and we keep 20% of the resultant disk flux as the thermal component.

Table 2. Input parameters for the standard model.

Parameter	Adopted value
cell resolution	12.2 pc
HI half thickness	180 pc
H ₂ scaleheight	65 pc
mean V _{OB}	10 kms ⁻¹
n _γ	100
time step	10 ⁶ years
number of molecular clouds	18000
number of OB associations	12000
star formation rate (2 – 60 M _⊙)	4.0 M _⊙ yr ⁻¹
volume filling factor of H ₂	2.5 %

Table 3. Output values from the simulation for the standard model.

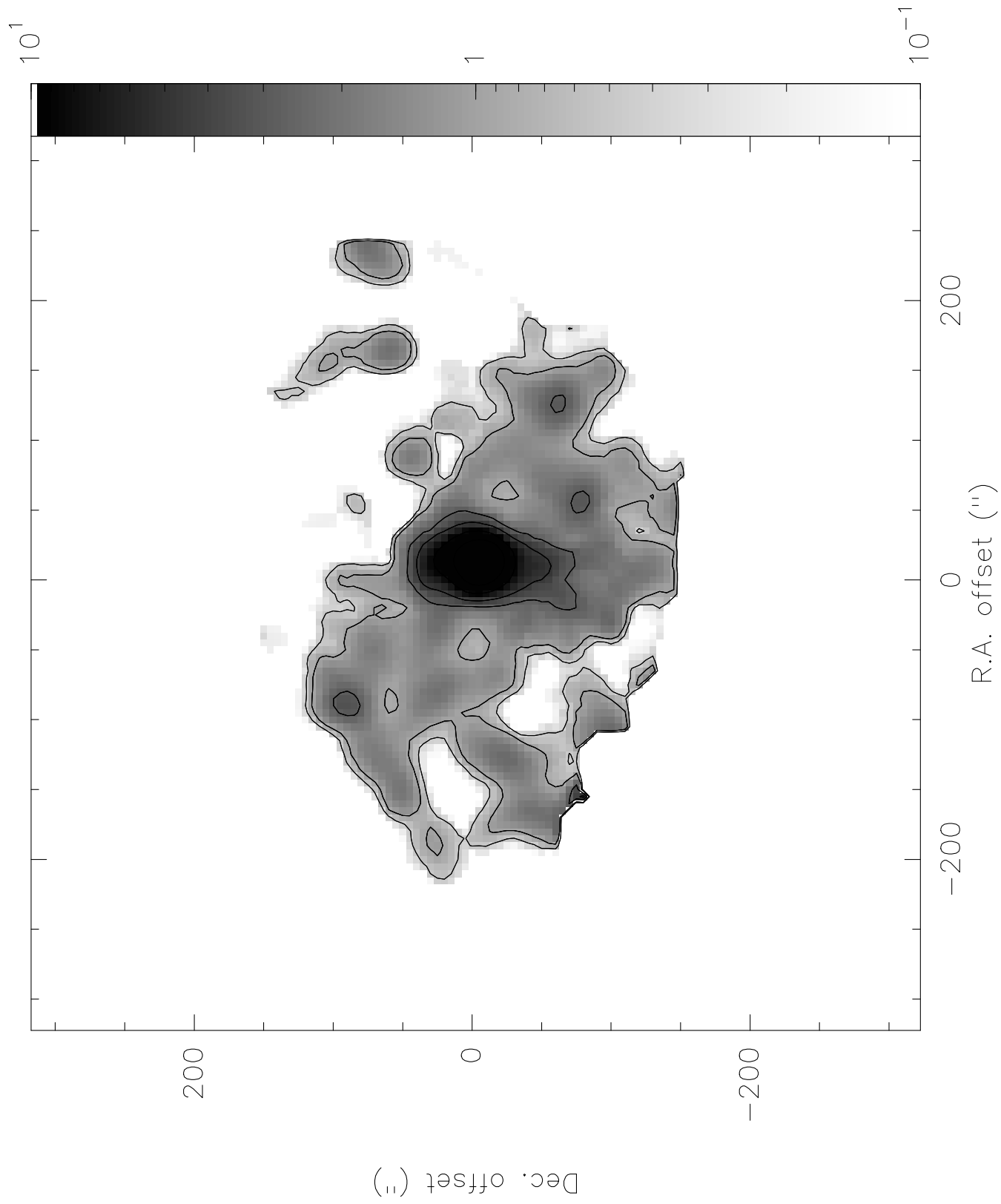
Parameter	Total	Dense	Diffuse	UV	ISRF
L _{912–2000Å} (L _⊙)	1.3 10 ¹⁰	—	—	—	—
L _{1950–2050Å} (L _⊙)	5.2 10 ⁸	—	—	—	—
L _{Hα} (L _⊙)	1.2 10 ⁸	—	—	—	—
B _t ⁰ (mag)	8.96	—	—	—	—
L ₁₂ (L _⊙)	2.1 10 ⁹	1.0 10 ⁹	1.0 10 ⁹	1.7 10 ⁹	0.3 10 ⁹
L ₂₅ (L _⊙)	2.0 10 ⁹	1.0 10 ⁹	1.0 10 ⁹	1.7 10 ⁹	0.3 10 ⁹
L ₆₀ (L _⊙)	5.1 10 ⁹	2.9 10 ⁹	2.2 10 ⁹	4.2 10 ⁹	0.9 10 ⁹
L ₁₀₀ (L _⊙)	8.5 10 ⁹	4.5 10 ⁹	4.0 10 ⁹	6.1 10 ⁹	2.4 10 ⁹
L ₂₀₀ (L _⊙)	4.9 10 ⁹	2.5 10 ⁹	2.5 10 ⁹	3.0 10 ⁹	1.9 10 ⁹
L _{60–200} (L _⊙)	18.6 10 ⁹	9.9 10 ⁹	8.6 10 ⁹	13.3 10 ⁹	5.2 10 ⁹
L _{C+} (L _⊙)	2.6 10 ⁷	2.0 10 ⁷	0.6 10 ⁷	—	—
S _{6cm} (mJy)	124	—	—	—	—
L _{C+} /L _{FIR} (60–100)	0.18 %	0.25 %	0.10 %	—	—

All luminosities are emergent luminosities. The total UV luminosity generated by OB associations in the disk between 912 and 2000 Å is 3.10×10^{10} L_⊙.

References

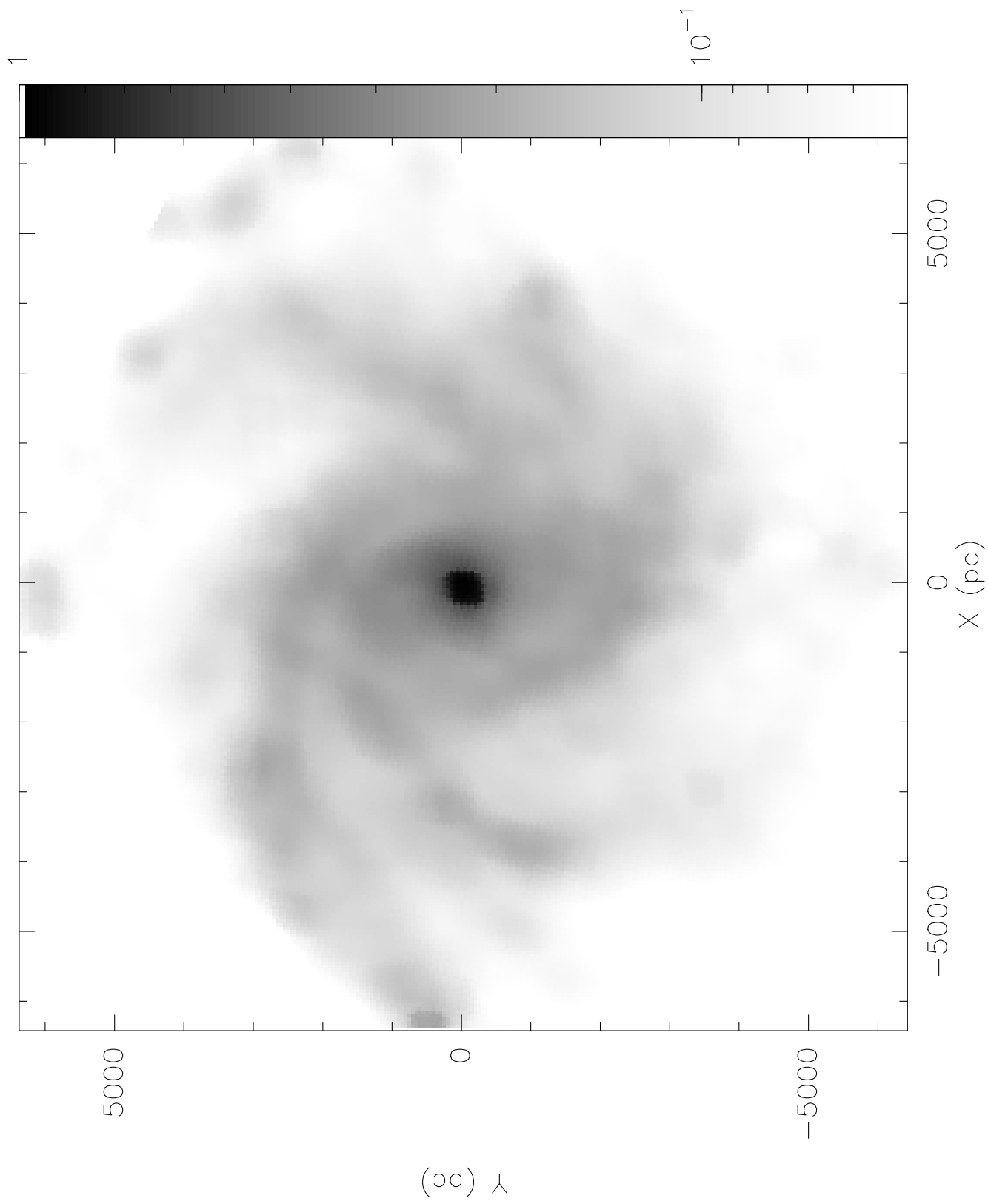
- Bohlin R.C., Savage B.D., Drake J.F., 1978, ApJ 224, 132
 Bonnarel F., Boulesteix J., Georgelin Y.P. et al., 1988, A&A 189, 59
 Boulanger F., Viallefond F., 1992, A&A 266, 37
 Boulanger F., Abergel A., Bernard J.P. et al., 1996, A&A 312, 256
 Bruzual A.G., Magris G., Calvet N., 1988, ApJ 333, 673
 Buat V., Xu C., 1996, A&A 306, 61
 Buat V., Deharveng J.M., Donas J., 1989, A&A 223, 42
 Calzetti D., Kinney A.L., Storchi-Bergman T., 1995, ApJ 429, 582
 Casoli F., Clausset F., Viallefond F., Combes F., Boulanger F., 1990, A&A 233, 357
 Caux E., Puget J.L., Serra G., Gispert R., Ryter C., 1985, A&A 144, 37
 Clausset F., Casoli F., Viallefond F., Combes F., 1991, in *Dynamics of galaxies and their molecular cloud distribution*, F. Combes, F. Casoli eds, p. 88
 Combes F., Gerin M., 1985, A&A 150, 327
 Considère S., Athanassoula E. 1988, A&AS 76, 365
 Cox P., Mezger P.G., 1989, A&AR 1, 49
 Cox P., Krügel E., Mezger P.G., 1986, A&A 155, 380
 DeGioa-Eastwood K., et al., 1984, ApJ 278, 564
 Désert F.X., Boulanger F., Puget J.L., 1990, A&A 237, 215
 Devereux N.A., Young J., 1990, ApJ 350, L25
 de Vaucouleurs G., 1979, ApJ 227, 380
 Donas J., Deharveng J.M., 1987, A&A 180, 12
 Engargiola G., 1991, ApJS 76, 875
 Falgarone E., Puget J.L., Pérault M., 1992, A&A 257, 715
 Fitzpatrick E.L., Massa D., 1988, ApJ 328, 734
 Garcia-Burillo S., Combes F., Gerin M., 1993, A&A 274, 148
 Garmany C.D., 1994, PASP 106, 25
 Gerin M., Casoli F., Combes F., 1991, A&A 251, 32
 Güsten R., Mezger P., 1983, Vistas in Astronomy 26, 159
 Helou G., Malhotra S., Beichman C.A. et al., 1996, A&A 315, L157
 Henyey L.G., Greenstein J.L., 1941, ApJ 93, 70
 Heydari-Malayeri M., Beuzit J.L., 1994, A&A 287, L17
 Hippelein H., Lemke D., Haas M. et al., 1996, A&A 315, L82
 Jaffe D.T., Zhou S., Howe J.E. et al., 1994, ApJ 436, 203
 Kennicutt R., 1989, ApJ 344, 685
 Klein U., Beck R., Buczilowski U.R., Wielebinski R., 1982, A&A 108, 176
 LeBourlot J., Pineau des Forêts G., Roueff E., 1993, A&A 267, 233
 Leisawitz D., 1991, ApJS 77, 451
 Leisawitz D., Hauser M.G., 1988, ApJ 332, 954
 Leisawitz D., Bash F.N., Thaddeus P., 1989, ApJS L. 70, 731
 Li, Li, 1995, A&A 301, 666
 Lord S.D., Malhotra S. et al., 1996, A&A 315, L117
 Lu N.Y., Helou G., Tuffs R. et al., 1996, A&A 315, L153
 Mc Kee C.F., Williams J.B., 1997, ApJ 476, 144
 Madden S., Geis N., Genzel R. et al., 1993, ApJ 407, 579
 Madden S., Geis N., Genzel R. et al., 1994, Infrared Phys. Technol. 35, no 2/3, 311
 Malhotra S., Helou G., Van Buren D. et al., 1996, A&A 315, L161
 Martin P., 1995, AJ 109, 2428
 Massey P., Johnson K.E., De Gioa-Eastwood K., 1995, ApJ 454, 151
 Mathis J.S., Mezger P.G., Panagia N., 1983, A&A 128, 212
 Mezger P., 1972, in *Interstellar matter*, editors W.C. Wickramasinghe, F.D. Kahn and P.G. Mezger
 Miller W.W. III., Cox D.P., 1993, ApJ 417, 579
 Murthy J., Walker H.J., Henry R.C., 1992, ApJ 401, 574
 Myers P.C., Dame T.C., Thaddeus P. et al., 1986, ApJ 301, 398
 Osterbrock D.E., 1989, in *Astrophysics of Gaseous Nebulae and Active Galactic Nuclei*, University Science Books
 Peimbert M., Rayo J.F., Torres-Peimbert S., 1975, Revista Mexicana de Astronomia y Fisica 1, 289
 Rifatto A., Longo G., Capaccioli M., 1995, A&AS 114, 527
 Rice W., Boulanger F., Viallefond F., Soifer B.T., Freedman W.L., 1990, ApJ 358, 418
 Rubio M., Lequeux J., Boulanger F. et al., 1993, A&A 271, 1
 Ryter C., Puget J.L., Pérault M., 1987, A&A 186, 312
 Seaton M.J., 1979, MNRAS 187, 73
 Shibai H., Okuda H., Nakagawa T. et al., 1991, ApJ 374, 522
 Snow T.P., Witt A., 1996, ApJ 468, L65

- Solomon P., Sanders D., Rivolo A.R., 1985, ApJ 292, L19
Thronson H.A., Majewski S., Descartes L., Hereld M., 1990, ApJ 364, 456.
Tielens A. G. G. M., Hollenbach D., 1995, ApJ 291, 747
Tuffs R., Lemke D., Xu C. et al., 1996, A&A 315, L149
Turner J.L., Ho P., 1994, ApJ 421, 122
van der Hulst J.M., Kennicutt R.C., Crane P.C., Rots A.H., 1988, A&A 195, 38
Walterbos R.A.M., Greenawalt B., 1996, ApJ 460, 696
Williams J., McKee C., 1997, ApJ 476, 166
Witt A., 1977, ApJS 35, 1
Witt A., Gordon K.D., 1996, in *Unveiling the Cosmic Infrared Background*, E. Dwek ed., AIP Conf. Proc 348
Wolfire M.G., Hollenbach D., McKee C.F., Tielens A.G.G.M., Bakes E.L.O., 1995, ApJ 443, 152
Wright E.L., Mather J.C., Bennett C.L. et al., 1991, ApJ 381, 200
Wyse R.F.G., Silk J., 1989, ApJ 339, 700
Young J., Scoville N., 1982, ApJ 258, 476
Young J., Allen L., Kenney J.D.P., Lesser A., Rownd B., 1996, AJ 112, 1903



This figure "0714-f2.jpeg" is available in "jpeg" format from:

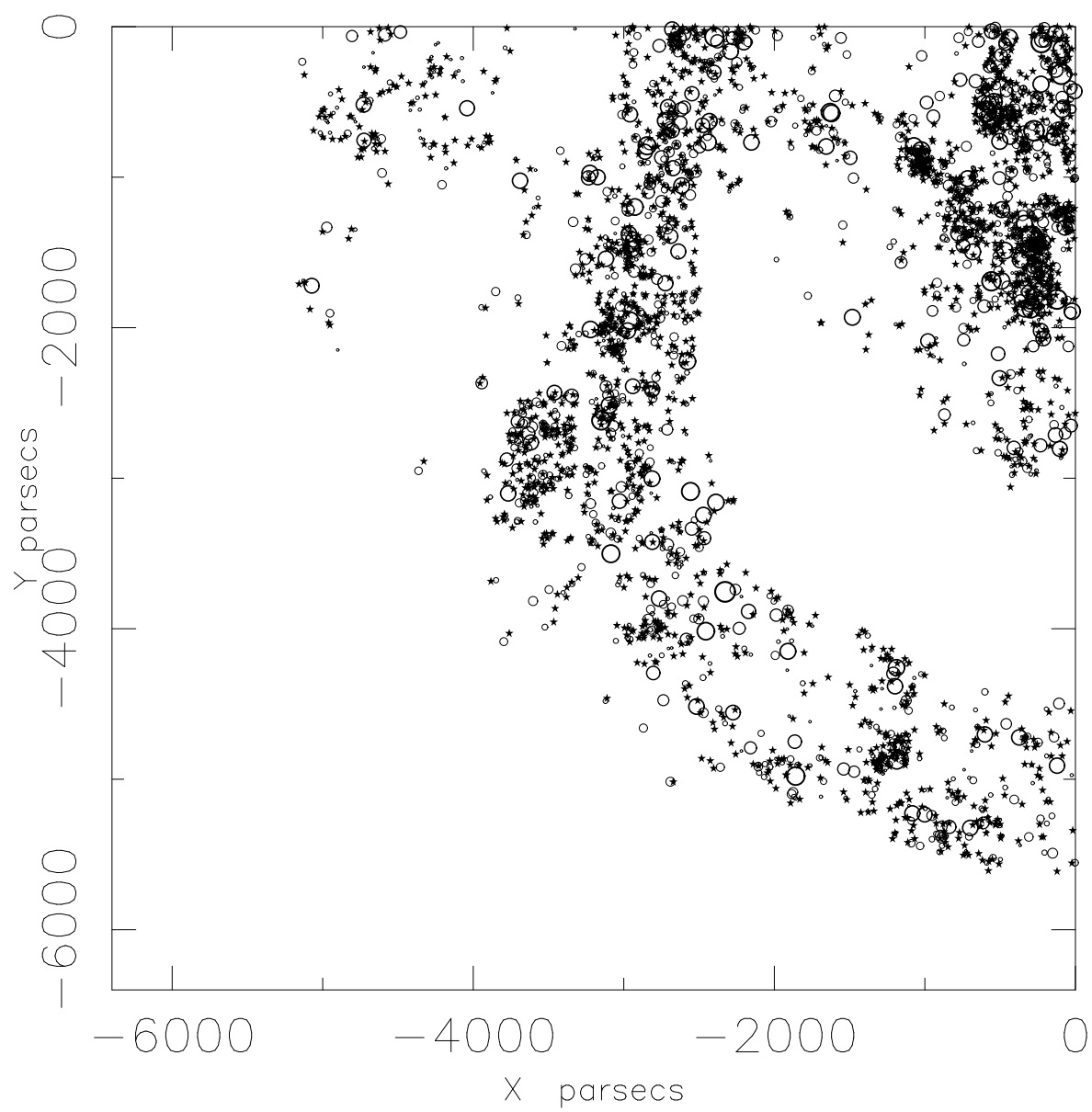
<http://arxiv.org/ps/astro-ph/9806214v1>

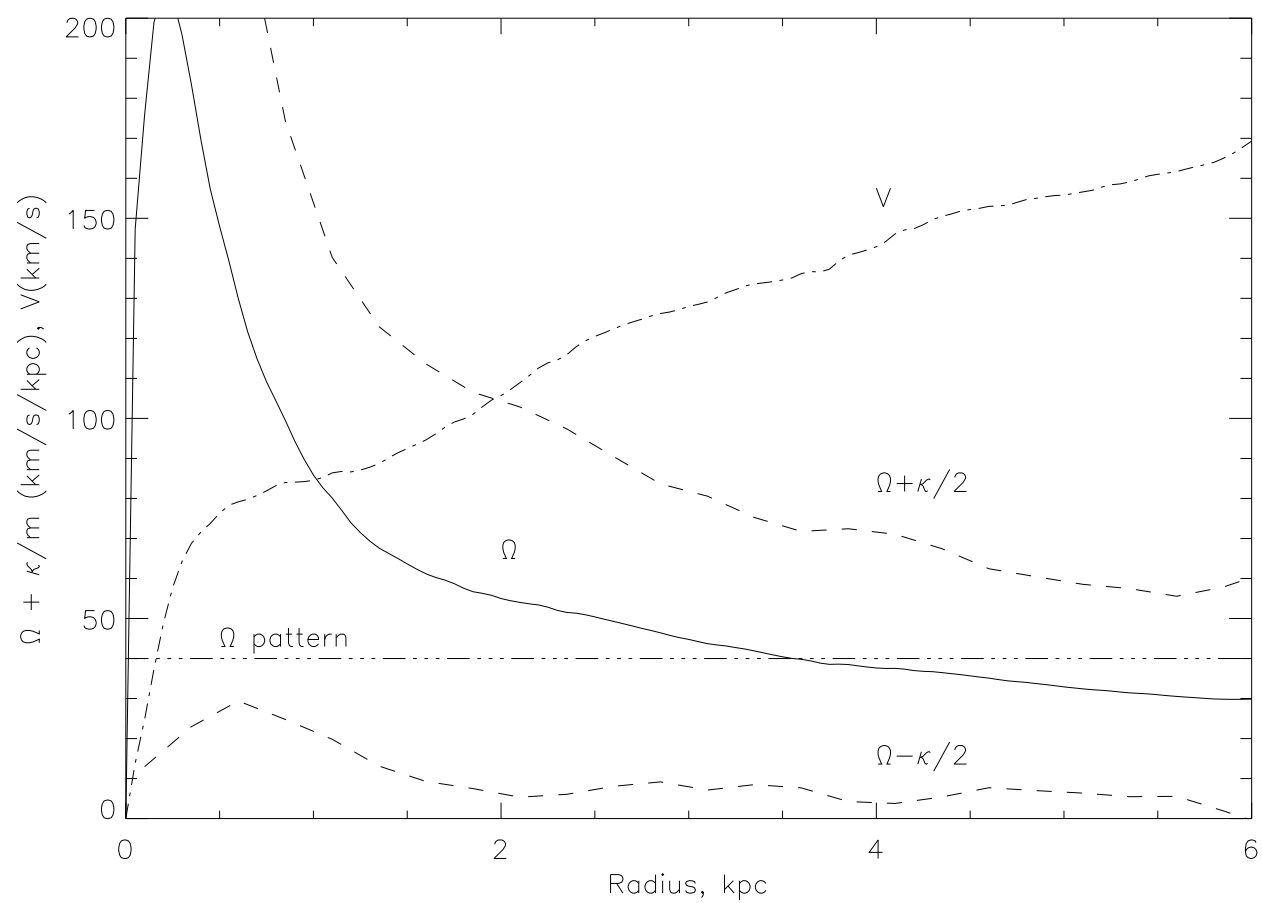


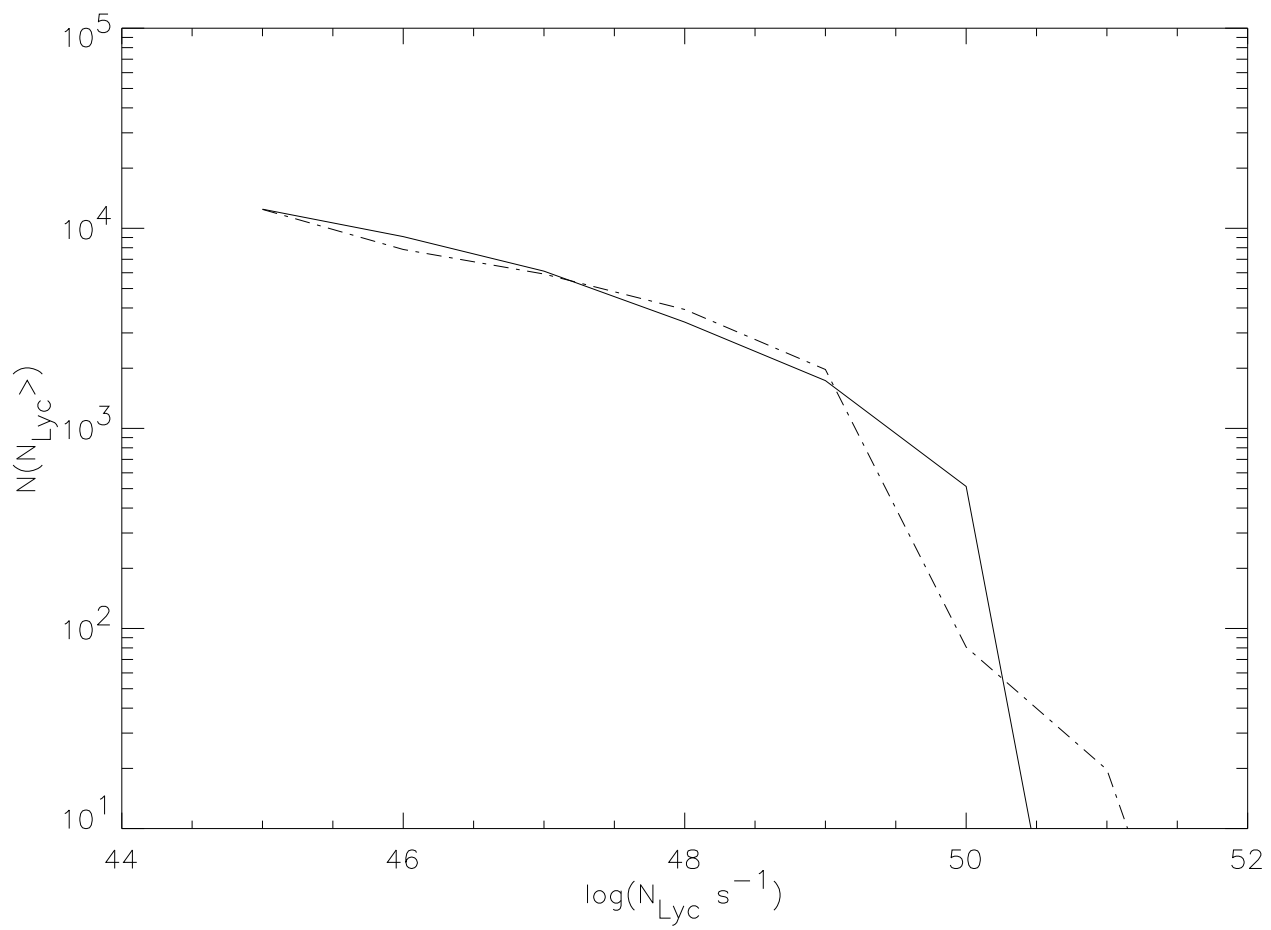
This figure "0714-f3b.gif" is available in "gif" format from:

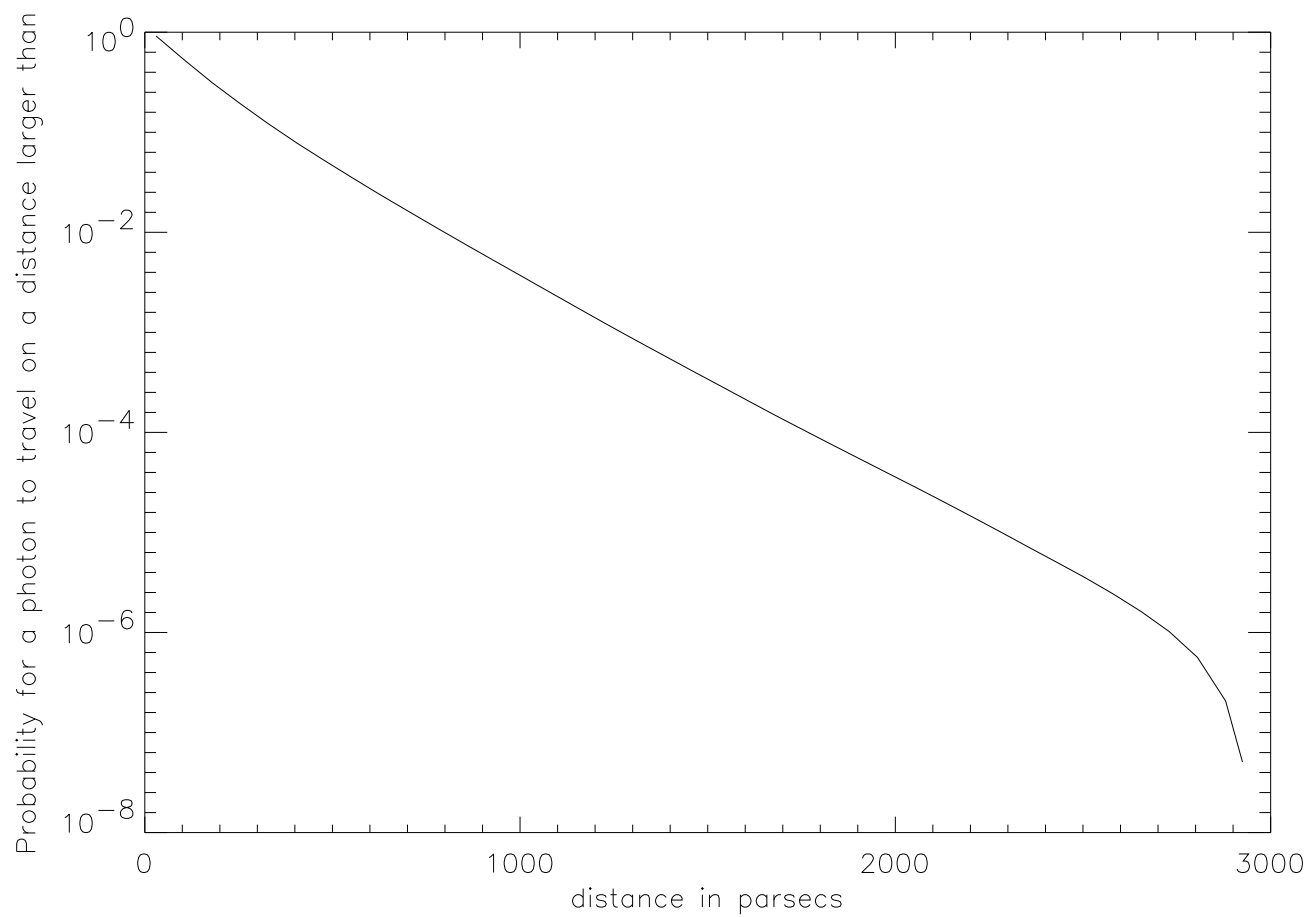
<http://arxiv.org/ps/astro-ph/9806214v1>

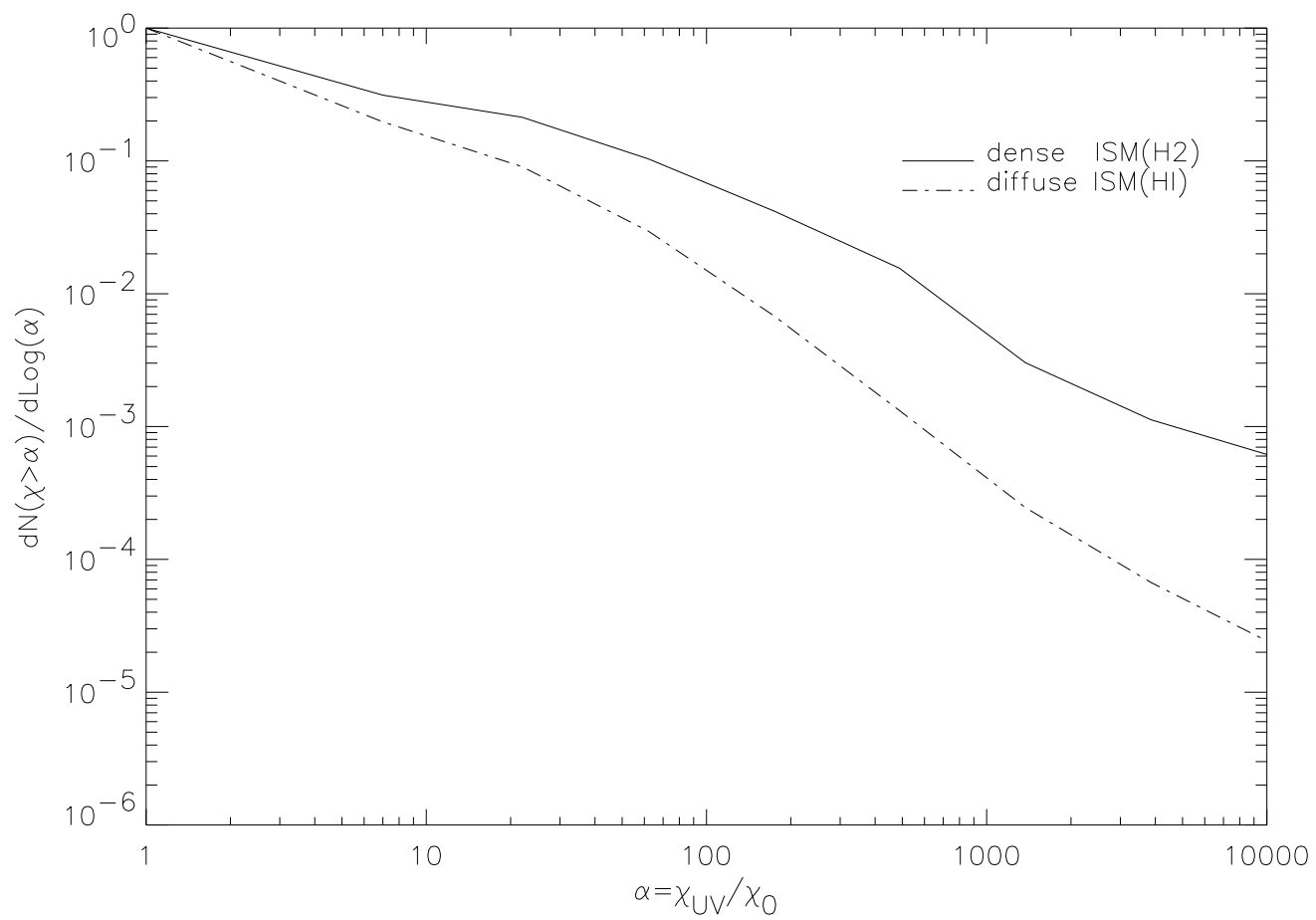
NGC 6946: molecular clouds

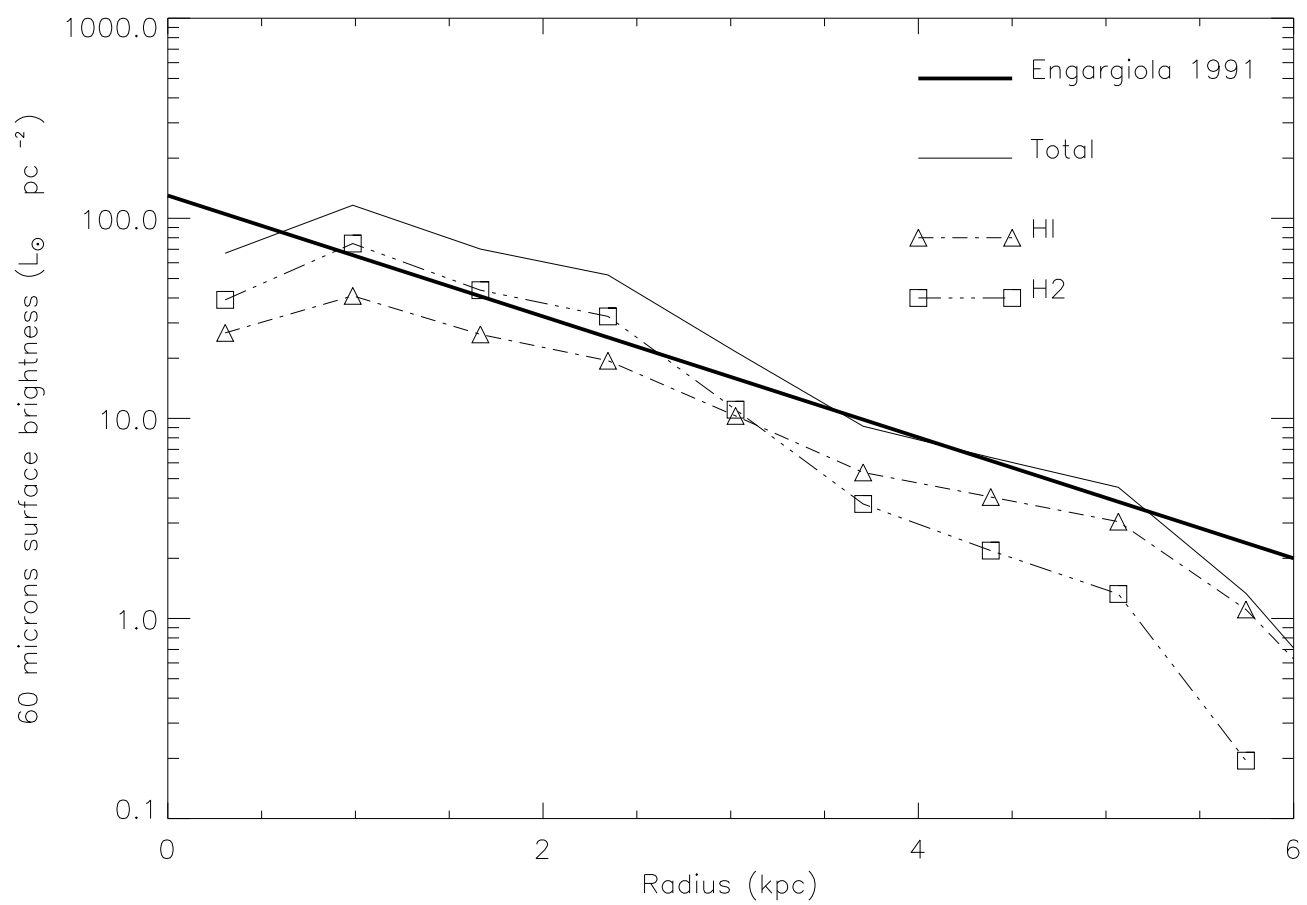


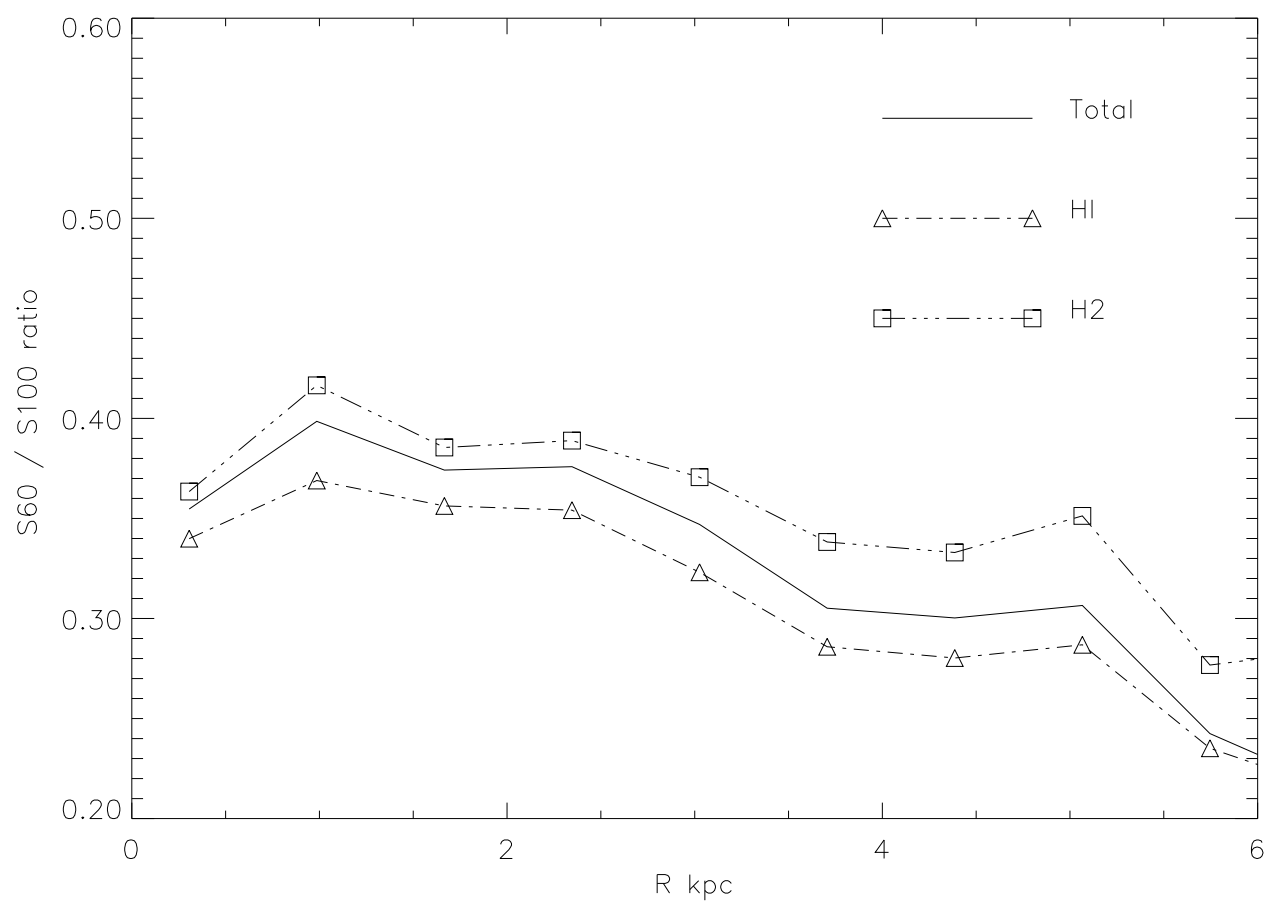


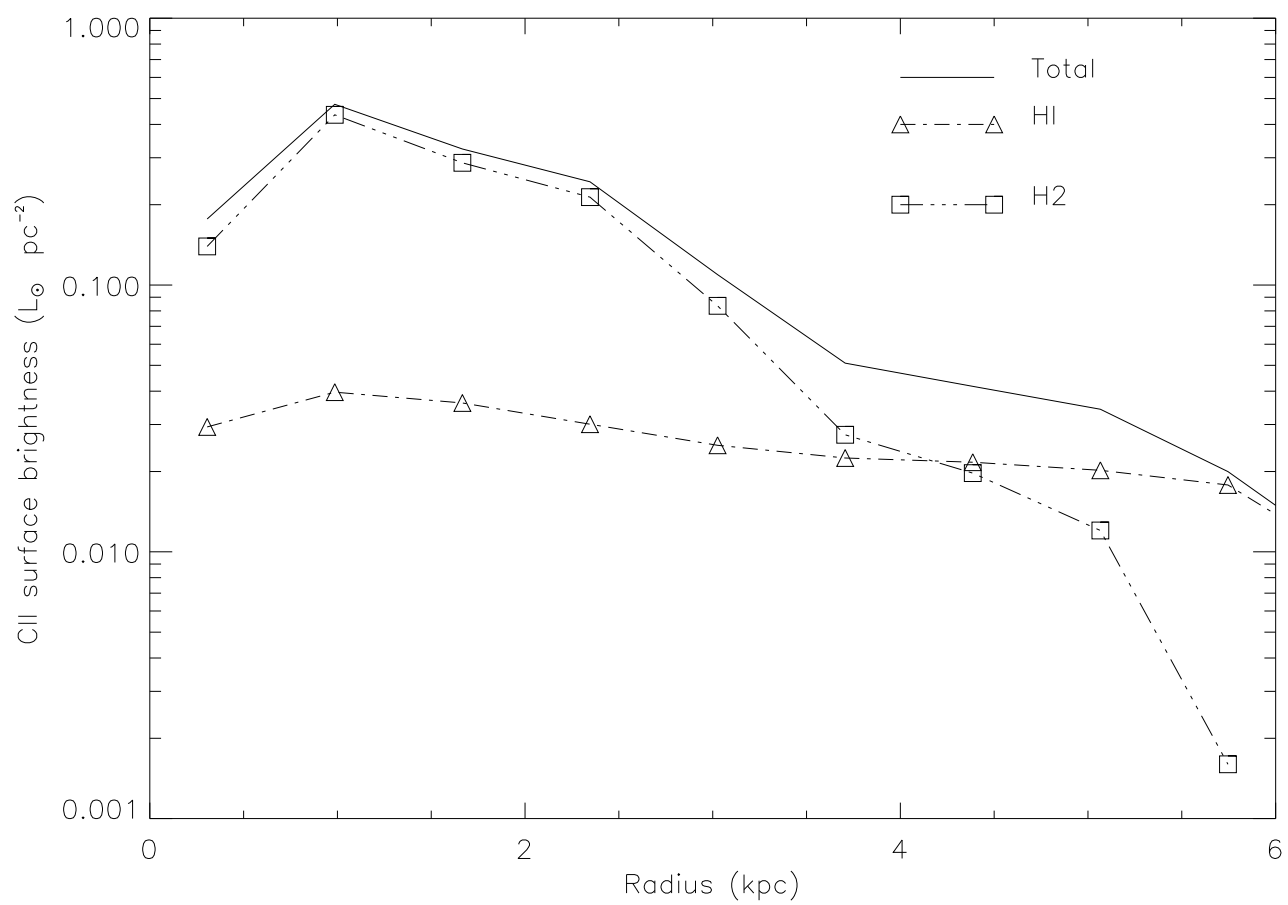


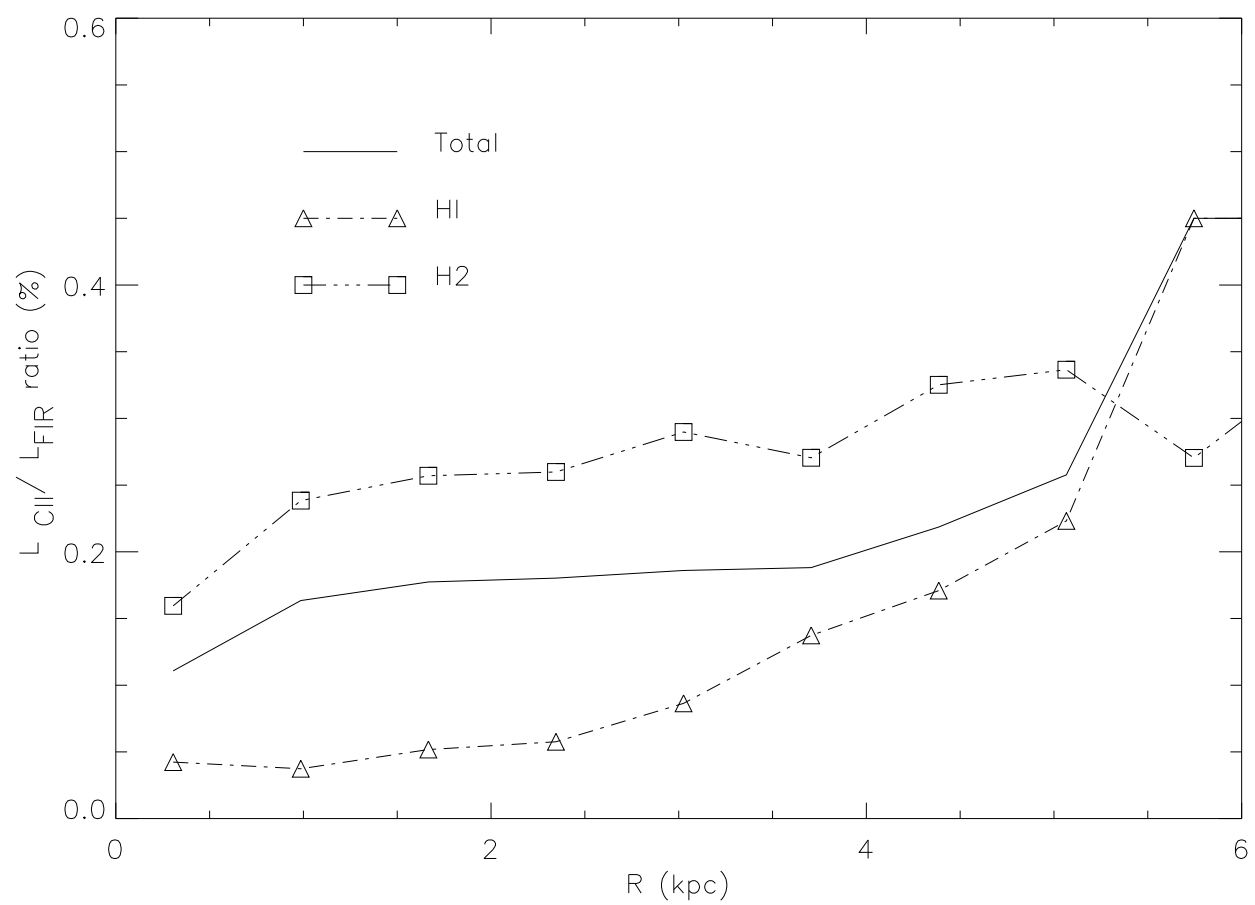


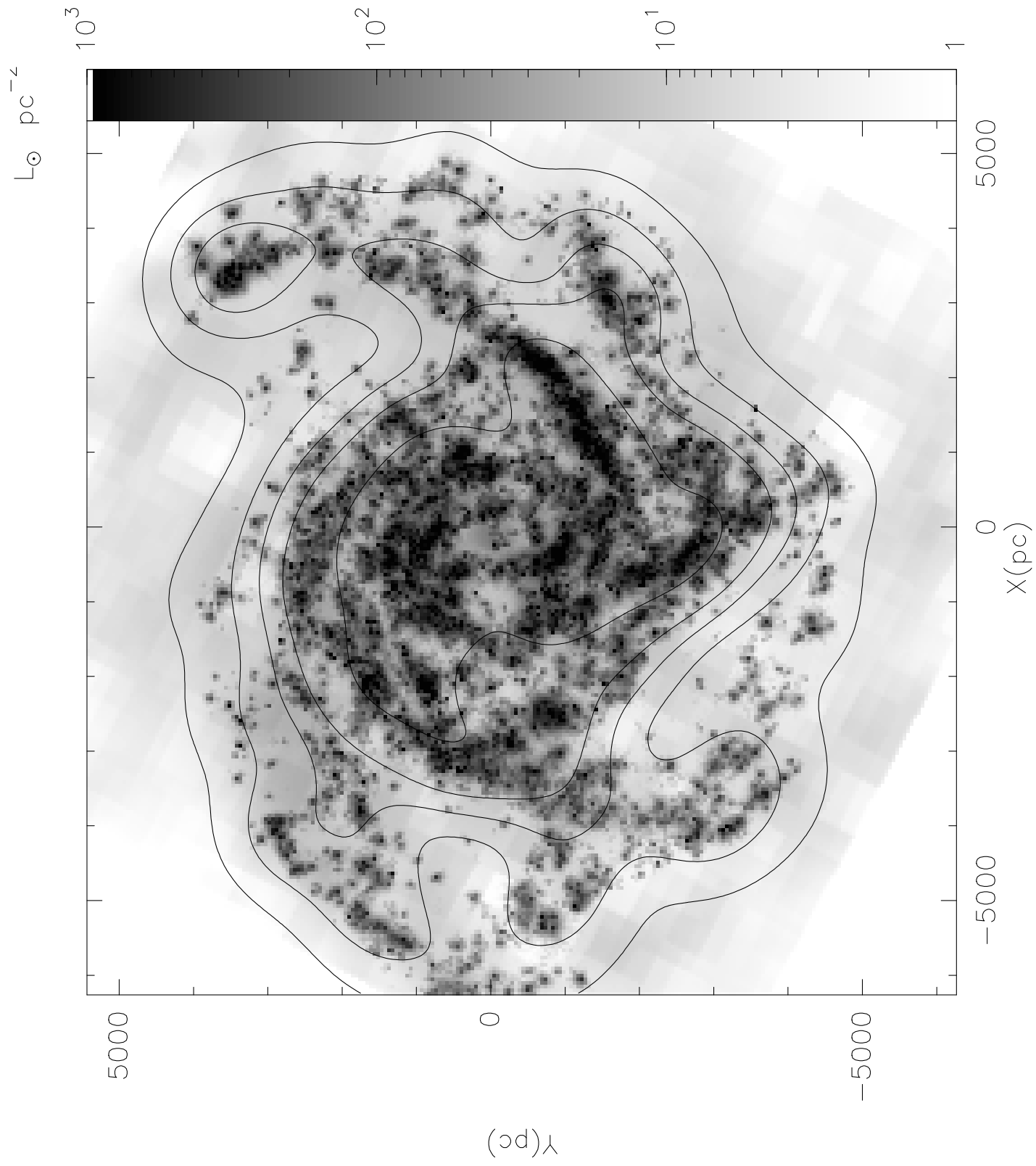


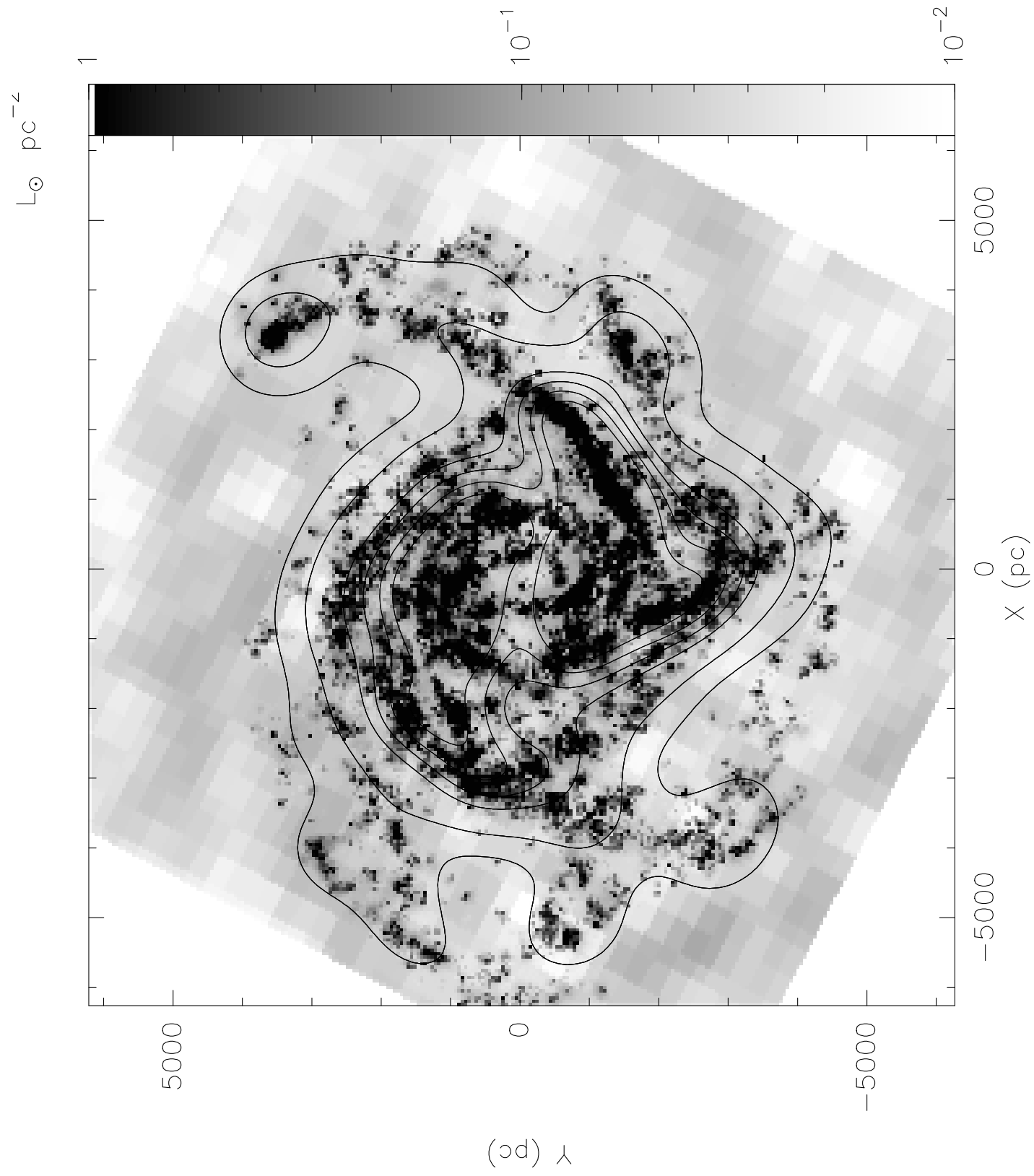




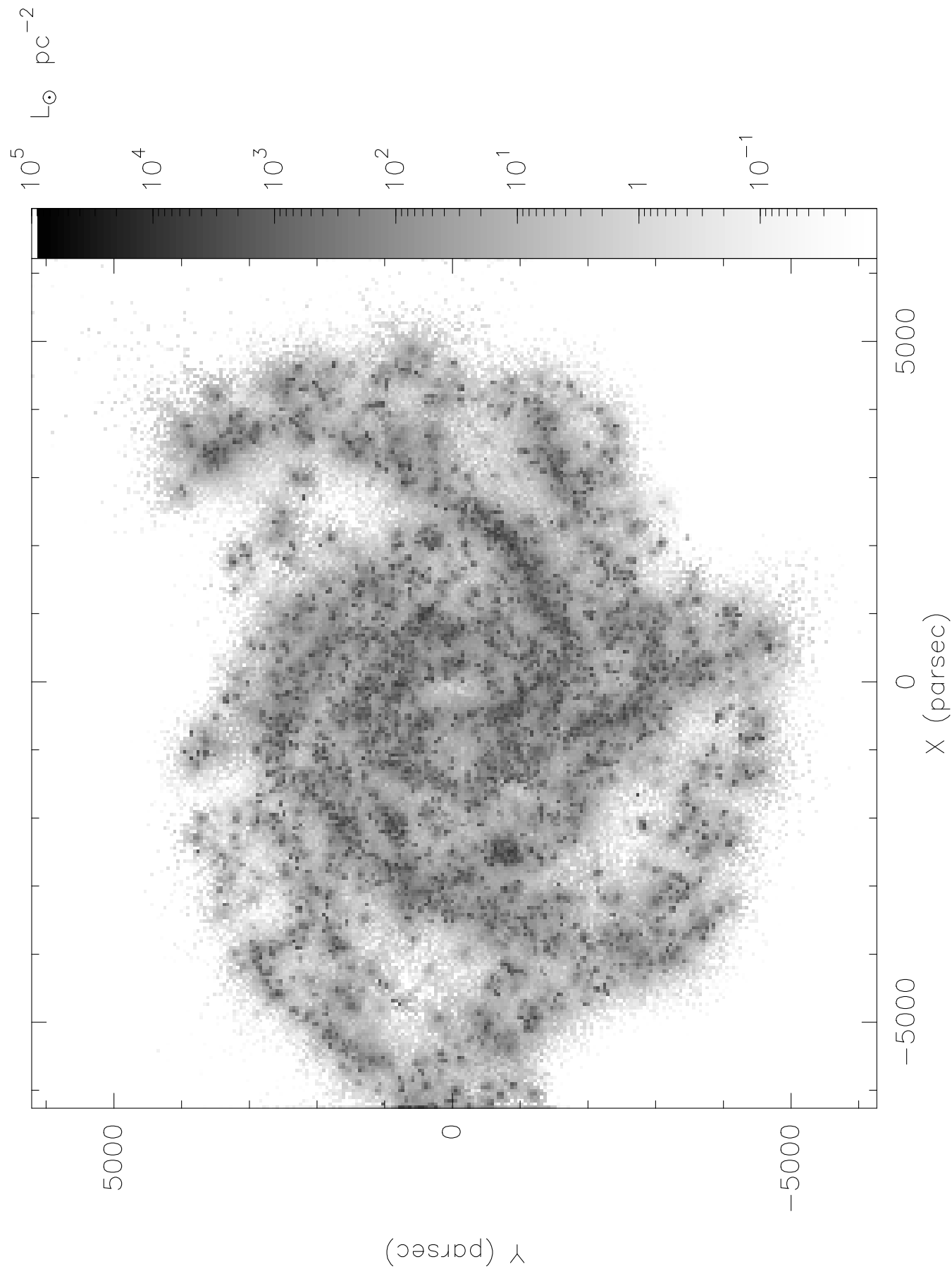




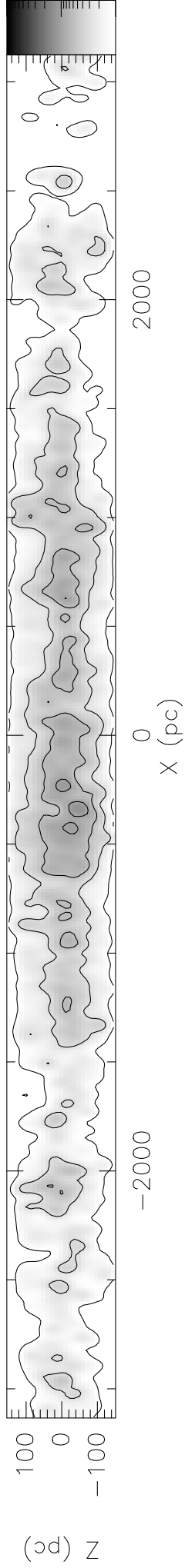


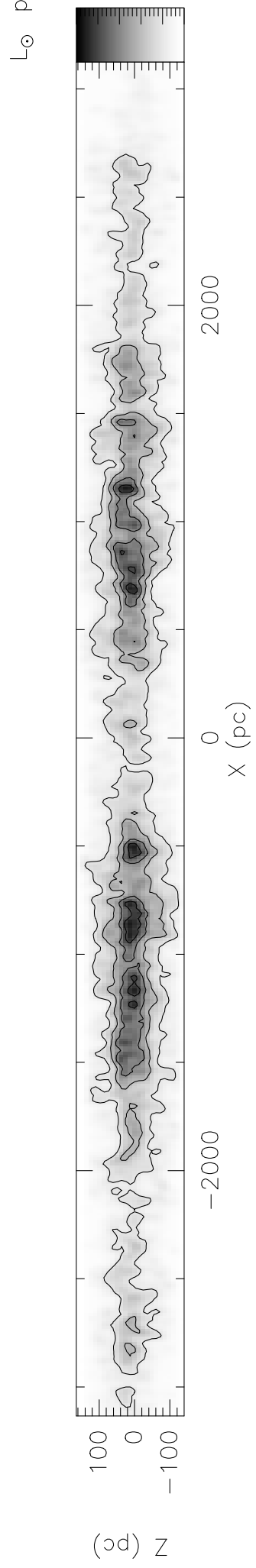


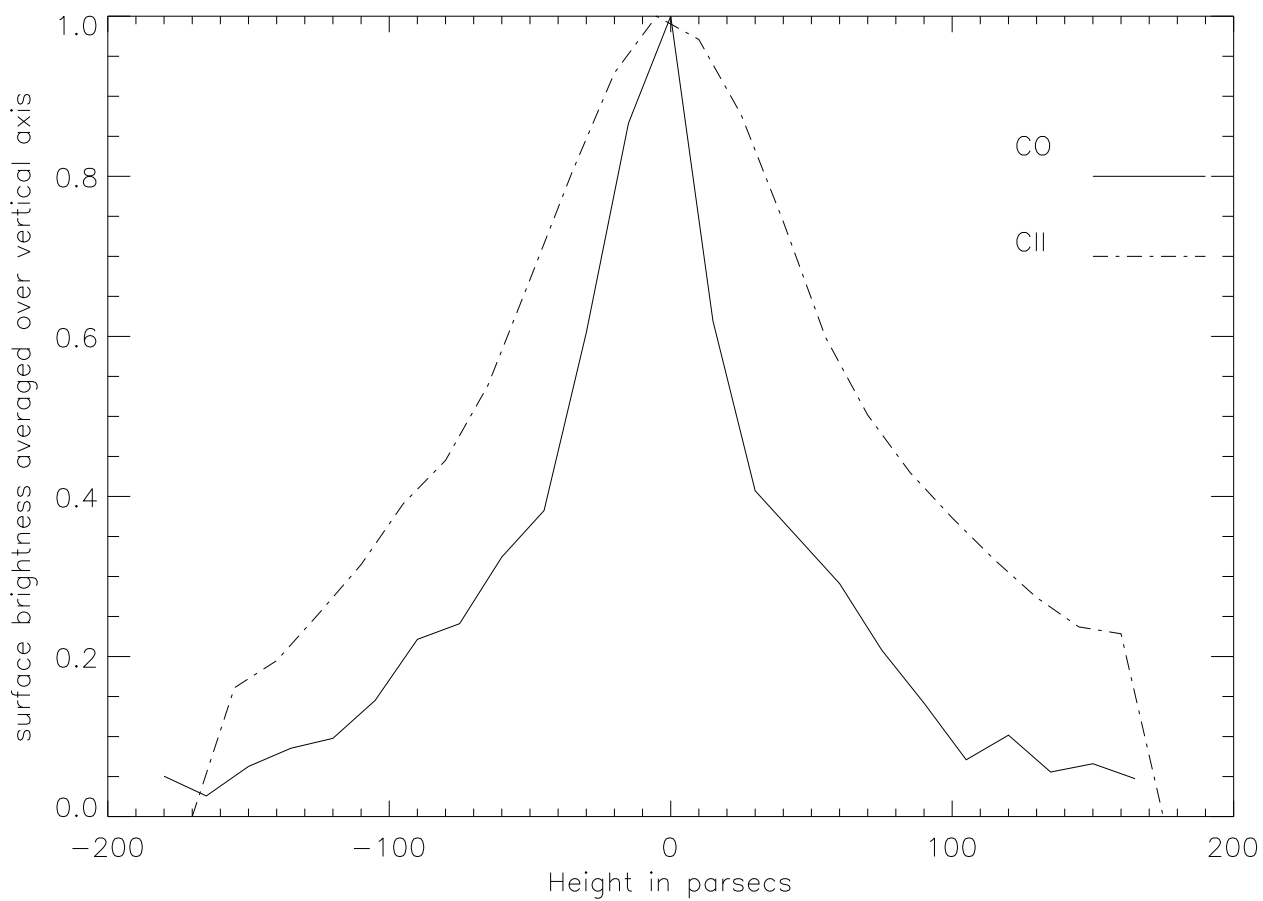
UV (912–2000 Å) surf. brightness



$L_{\odot} \text{ pc}^{-2}$







FIR and C⁺ emissions of spiral galaxies disks.

The example of NGC 6946.

S. Sauty¹, M. Gerin^{2,1}, F. Casoli¹

¹ DEMIRM, Observatoire de Paris, 61 Av. de l'Observatoire, 75014 Paris, France; and URA 336 du CNRS

² Radioastronomie Millimétrique, ENS, 24 Rue Lhomond, 75231 Paris Cedex 05, France; and URA 336 du CNRS

Received 15 October 1997; accepted 25 May 1998

Abstract. We present numerical simulations of radiative transfer in the spiral galaxy NGC 6946. The interstellar medium is represented as a two phases medium, with molecular clouds and a smooth diffuse phase. The molecular gas distribution is calculated in a self-consistent way from the distribution of an ensemble of molecular clouds evolving in the gravitational potential of NGC 6946. We simulate star formation by creating OB associations in molecular clouds. The transfer of UV radiation is calculated in the clumpy interstellar medium, to determine the local UV illumination of molecular clouds. We compute the emergent intensity in the UV continuum (912 – 2000 Å), in the H α and C⁺ $^2P_{3/2} - ^2P_{1/2}$ lines as well as in the continuum at far infrared wavelengths, 60, 100 & 200 μ m.

It is possible to obtain a consistent picture of this galaxy with a global star formation rate of 4 M $_{\odot}$ yr⁻¹ (for stars with masses in the range 2-60 M $_{\odot}$) occurring mostly in the spiral arms. The close spatial association of massive stars and molecular clouds has a profound impact on the transfer of UV radiation in the galactic disk and on the dust emission. The median distance travelled by UV photons is about 120 pc. However, when they have escaped from the vicinity of their parent OB associations, UV photons may travel quite far in the disk, up to 1 kpc. The UV opacity of the model spiral galaxy disk, observed face-on, is 0.8 at 1000 Å and 0.7 at 2000 Å.

For radii less than 4 kpc, the C⁺ 158 μ m line is mostly produced in photodissociation regions at the surfaces of molecular clouds. The C⁺ emission from diffuse atomic gas accounts for about 20% of the total. It becomes significant at large distance from the nucleus ($r \geq 4$ kpc). Molecular clouds and diffuse atomic gas have almost equal contributions to the total far infrared emission from 60 to 200 μ m. As a whole, 72% of the 60 – 200 μ m FIR emission can be attributed to dust grains heated by the UV radiation of massive stars and 28% by the radiation field

of the old stellar population.

Key words: Galaxies : ISM, Galaxies : individual: NGC 6946, – ISM : molecules, ISM : dust

1. Introduction

Because the peak of the thermal dust emission occurs in the far-infrared (60-200 μ m) for Galactic interstellar clouds, this wavelength domain is recognized as a very important ‘window’ to study the interstellar medium, both in the Milky Way and in external galaxies. However, due to the lack of spatial resolution provided by telescopes operating at these wavelengths, the interpretation of the signals measured in external galaxies is still a subject of controversy. The debate is focussed on the origins of the heating of dust grains and of the $^2P_{3/2} - ^2P_{1/2}$ C⁺ line at 158 μ m. This fine structure line of ionized carbon is one of the main cooling lines of neutral atomic gas (Wolfire et al. 1995), but it is also seen in HII regions, with different excitation mechanisms in these two cases. Other sources of C⁺ emission are the dense photodissociation regions (PDRs) where intense UV radiation from massive stars impinges on molecular clouds. In these regions, the photodissociation of carbon monoxide creates a layer of ionized carbon at the edge of the molecular cloud, which is a source of intense C⁺ emission.

The far infrared emission is produced by dust grains heated by star light but the relative contribution of young massive stars on one hand, and of the bulk of the stellar population on the other hand, are still debated (see e.g. Walterbos & Greenawalt 1996, Devereux & Young 1990, Cox & Mezger 1989, Thronson et al. 1990, Rice et al. 1990). Using low resolution data from IRAS, IR colors have been used to assess the respective roles of star

forming regions and cirrus in external galaxies at a global scale (e.g. Calzetti et al. 1995). It is difficult to find spiral galaxies dominated by a single population of heating sources, since the relative contributions of massive stars and of the disk population vary from galaxy to galaxy, and probably from place to place in a given galaxy. A main problem of these studies is the lack of spatial resolution at far infrared wavelengths. Even when it is possible to use high spatial resolution data at millimeter and sub-millimeter wavelengths, the gap in spatial resolution from the local interstellar clouds to external galaxies is huge: for nearby galaxies located at distances D of a few Mpc, a one arcmin beam encompasses $0.3(D/1\text{Mpc})\text{kpc}$, much larger than the size of a single molecular complex in the Galaxy, whereas structures down to 0.01 pc are commonly observed in local clouds (Falgarone et al. 1992) and in the Magellanic Clouds (Rubio et al. 1993).

Numerical simulations provide a way out of this problem: it is possible to reproduce the observed molecular gas distribution of nearby spiral galaxies with numerical simulations using observed data as input parameters. For example Garcia-Burillo et al. (1993) were able to fit the spatial distribution and kinematics of the molecular gas in M 51 using the cloud collision code developed by Combes & Gerin (1985). Though this code has a spatial resolution of a few hundred parsecs (the cell size for the large scale dynamics), it is possible to include "micro-physics" at the parsec scale inside each cell. We have taken this approach and implemented star formation in this code to study the far infrared and C⁺ emissions in the spiral galaxy NGC 6946. The next section summarizes the current data on NGC 6946. We describe the model in Sect. 3 and present the results for NGC 6946 in Sect. 4. The implications of this work for the interpretation of the C⁺ and FIR emission of spiral galaxies are discussed in Sect. 5.

2. NGC 6946

NGC 6946 is a nearby Scd galaxy with a low inclination, $i = 34^\circ$ (Considère & Athanassoula 1988). At the adopted distance of 5 Mpc, 1 arcmin on the sky corresponds to a linear size of 1.5 kpc. The main characteristics of NGC 6946 are summarized in Table 1. It shows a weak bar (Martin 1995) and a prominent spiral structure with both an $m = 2$ and an $m = 4$ pattern (Considère & Athanassoula 1988). With this open spiral structure, the arm and interarm regions are resolved at moderate spatial resolution (30"). The gas distribution is well known since NGC 6946 has been mapped at high spatial resolution in HI (Boulanger & Viallefond 1992), and CO (Casoli et al. 1990, Clausset et al. 1991). Figure 1 presents a CO(2-1) map obtained at the IRAM 30m telescope (Clausset et al. 1991), and Fig. 2 a V-I color map obtained at the Observatoire de Haute-Provence (OHP) (P. Boissé, private communication). NGC 6946 is marginally resolved in the far infrared maps obtained by IRAS and the KAO (Engar-

giola 1991). It also belongs to the normal galaxy sample studied by ISO and as such has been extensively mapped in the mid and far infrared (Malhotra et al. 1996, Helou et al. 1996, Lu et al. 1996, Tuffs et al. 1996). NGC 6946 is forming stars actively, as revealed by its bright H α emission (Bonnarel et al. 1988a, 1988b, Kennicutt 1989) and the numerous supernovae (Li & Li 1995). Madden et al. (1993) have mapped the C⁺ 158 μm emission at 45" resolution with the KAO. Bright C⁺ emission is found in the nucleus and in the disk. At this scale, the C⁺ emission is correlated with the CO emission in the spiral arms and with the HI emission in the outer disk.

3. A model of NGC 6946

3.1. Representation of the interstellar medium.

We have chosen to include two phases for the interstellar medium :

- i) a dense molecular phase composed of spherical molecular clouds with masses ranging from 10^3 to $10^6 M_\odot$ and mean density $50 \text{ H}_2 \text{ cm}^{-3}$. This mean density is used to determine cloud sizes from their masses. The half power width of the molecular layer, defined as $\langle z^2 \rangle^{1/2}$, is equal to 65 pc. The global volume filling factor of this molecular phase in the disk, $\Phi_V(\text{H}_2)$, amounts to 2.5%. The clumpy structure of molecular clouds is taken into account by using a larger density, $5 \times 10^3 \text{ H}_2 \text{ cm}^{-3}$, to compute the C⁺ emission. The C⁺ emission is not sensitive to the gas density when it is larger than $\sim 10^3 \text{ cm}^{-3}$ (see Tielens & Hollenbach 1985 and Sect. 3.6). Indeed, C⁺ observations of nearby molecular clouds show that C⁺ emission is detected over the whole projected surface of molecular clouds (Jaffe et al. 1994). The total mass of dense molecular gas in the model is set to match the value deduced from CO(1-0) observations with a conversion factor of $2.3 \times 10^{20} \text{ H}_2 \text{ cm}^{-2} (\text{K kms}^{-1})^{-1}$, $2.0 \times 10^9 M_\odot$ (Table 1).
- ii) a neutral diffuse phase, with a nearly constant HI density. We have adjusted the value of the mean HI density using the data from Boulanger & Viallefond (1992): it varies slowly from 0.8 H cm^{-3} at the center to 2 H cm^{-3} in the outer disk ($r \sim 6 \text{ kpc}$). We have assumed that the HI disk has a vertical thickness of $360 \text{ pc} = 2H_z$, and that the density is uniform from $-H_z$ to $+H_z$. The velocity dispersion of the diffuse gas is set to 10 kms^{-1} . The total mass of diffuse neutral gas inside a radius of 6 arcmin is taken from the HI observations to be $2.6 \times 10^9 M_\odot$.

In addition to these two phases, we take into account the formation of HII regions around OB associations (see below). For the numerical calculations, we represent the galaxy disk as a large 3D grid. The total grid length L and the cell size r_{cell} are chosen to match the following constraints:

- the grid size has to be at least as large as the optical disk, which has a diameter of 12.5 kpc, in order to be able to follow the path of photons in the external regions of the

galaxy, and the heating of the neutral gas at large distance from the nucleus.

– the spatial resolution, r_{cell} , should be good enough to describe the clumpy structure of the medium: in particular the smallest clouds in the ensemble should occupy at least one cell. With the adopted parameters for the clouds, the radius of the smallest clouds with a mass of $10^3 M_\odot$ is 4.5 pc. This number is only an estimate of the actual size of a given cloud. It is possible to use an alternative method based on the scaling relations for molecular clouds, the so-called Larson’s laws. Using the mass-radius relation $M(M_\odot) = 100R^2(\text{pc}^2)$ (Falgarone et al. 1992), the radius of a $10^3 M_\odot$ cloud is then 3 pc. Another constraint on the spatial resolution is provided by the size of OB associations, which is generally larger than 30 pc (Garmany 1994) and their distance from molecular clouds. Leisawitz (1991) has estimated the mean distance between OB associations and their parent cloud to be about 50 parsecs.

We have chosen as the best compromise to represent the galaxy with a $1024 \times 1024 \times 24$ cell structure. The galaxy size is then $L = 2 \times R_{max} = 12.5$ kpc and the resolution $r_{cell} = 12.2$ pc. The cells are filled with neutral atomic gas, or with molecular gas at the molecular cloud positions, an $10^6 M_\odot$ molecular cloud then occupies $3 \times 3 \times 3$ cells. Finally, we include the ionized gas in the Strömgren spheres centered on each OB association, and replace the molecular and atomic gas with ionized gas whenever required. The radii of the Strömgren spheres are calculated assuming classical ionization in HII-bounded HII regions (Miller & Cox 1993). Because of the coarse spatial resolution of the dynamical code (200 pc), we do not attempt to reproduce the interstellar medium in the central region of NGC 6946 ($r < 500$ pc).

3.2. Spatial distribution of molecular clouds

This section of the code uses the cloud-cloud collision code described by Combes & Gerin (1985), and used by Garcia-Burillo et al. (1993) and Gerin et al. (1991) to model the gas dynamics in nearby galaxies. The molecular clouds move in the gravitational potential of the galaxy, they grow through cloud-cloud collisions, which are sticky processes, and are disrupted by simulated SN events. The molecular gas is immediately recycled into small molecular clouds. The gravitational potential is deduced from an R band image of NGC 6946 (Viallefond & Bonnarel, private communication, Bonnarel et al. 1988), with foreground stars removed. The image has been rotated to put the major axis vertical, and deprojected to face-on, using as projection parameters $PA = 69^\circ$ and $i = 34^\circ$. The image has then been binned to 256×256 pixels. This R band image covers $8.5' \times 8.5'$ on the sky, corresponding to a radius of 6.24 kpc at the assumed distance of NGC 6946, 5 Mpc. The actual spatial resolution amounts to a few times the cell size, about 200 pc. The following step is to build a good gravitational potential from this image.

As in Garcia-Burillo et al. (1993), the calculation is done in two steps. The axisymmetric part of the potential is obtained by assuming a constant mass to light ratio, and adjusting this constant to reproduce the observed CO and HI rotation curves. The perturbations due to the bar and spiral arms are included in the non axisymmetric part of the potential. The last parameter to adjust is Ω_p , the pattern speed of the density wave (bar + spiral arms). The gas distribution and velocity field are very sensitive to Ω_p . We find that $\Omega_p = 42 \text{ kms}^{-1} \text{ kpc}^{-1}$ gives the best results. The corotation is found at a radius of 3.5 kpc, close to the end of the bar, and the OLR lies outside of the disk. Figure 3a presents the deprojected R-band image. Figures 3b and 3c present an example of the obtained molecular cloud distribution. The gas clouds are concentrated in the spiral arms, with few molecular clouds at radii larger than 4 kpc. The model rotation curve is shown in Fig. 4, together with the angular frequency $\Omega(r)$. We have not attempted to model the compression of diffuse gas in the spiral structure, and have kept an axisymmetric distribution of diffuse atomic gas.

3.3. Stellar population

Once the gas is distributed over the galactic disk, we create OB associations, with star masses ranging from 10 to $60 M_\odot$ (stellar types from B2 to O5). We have chosen not to include stars less massive than $10 M_\odot$ because their lifetime becomes a significant fraction of the rotation period. Shortward of 2000 Å, the UV radiation is mostly produced by OB stars and the contribution by late B type stars is at most 20% (Walterbos & Greenawalt 1996, Mathis et al. 1983). The choice of the upper mass cutoff at $60 M_\odot$ is motivated by the work of Heydari-Malayeri & Beuzit (1994) who have shown that suspected very massive stars ($\sim 100 M_\odot$) are actually clusters of less massive stars. Also, a very short time step is required to sample adequately the lifetime of these very massive stars.

We allow only clouds more massive than $4 \times 10^4 M_\odot$ to form massive stars. In the cells satisfying this criterion, the OB associations are born at the outer edge of the molecular clouds. We have tested different star formation laws, so as to match as well as possible the H α radial profiles. The best fits are obtained with a star formation rate (SFR) depending on the angular frequency and the local gas surface density as proposed by Wyse & Silk (1989) :

$$SFR(r) = \epsilon \Omega(r) \sigma_{gas}(r)$$

with ϵ the star formation efficiency, $\Omega(r)$ the angular frequency at radius r and $\sigma_{gas}(r)$ the HI+H₂ surface density at position r in the disk. We find that $\epsilon = 5\%$ provides the best match to the H α radial profile by Kennicutt (1989).

The stellar mass distribution inside an OB association is drawn from the Initial Mass Function (IMF). We have chosen an index close to the Salpeter IMF, as suggested

by measurements in Galactic and extragalactic OB associations (Massey et al. 1995) : $\frac{dN(M)}{dM} = M^{-2.3}$.

The stellar associations are born with a mean velocity relative to their parent cloud chosen from a Gaussian of mean value 10 km s^{-1} and FWHM $\sim 10 \text{ km s}^{-1}$. These figures are in good agreement with observed data by Leisawitz et al. (1989) in their study of the relation of star clusters with molecular clouds. With this value, the average motion of OB stars relative to their parent cloud is 10 pc in 10^6 years. Finally, stars die after a time equal to their Main Sequence lifetimes from Güsten & Mezger (1983). Effective temperatures, stellar luminosities and radii, averaged over the main-sequence lifetime, are taken from Cox et al. (1986). Because we are only interested in broad band fluxes and colors, we have calculated all stellar fluxes, from UV to B bands, in the black-body approximation. Lyman continuum radiation production rates, averaged on the Main Sequence lifetime, are also taken from Cox et al. (1986) and Güsten & Mezger (1983) to have a coherent set of parameters. We use the parametrization as a function of the stellar mass, M :

$$\log_{10}\left(\frac{N_{Lyc}}{s^{-1}}\right) = 38.3 + 8.16 \times \log_{10}(M) - 0.24 \times \log_{10}^2(M) - 0.41 \times \log_{10}^3(M).$$

to compute the thermal radio continuum flux, H α luminosity and Strömgren sphere diameters.

We also include the effects of the radiation of massive stars on neutral gas, and allow molecular clouds to be partially eroded and ionized by the radiation of nearby OB associations, if they overlap with the Strömgren sphere of an OB association. We compute the radius of this sphere, R_{HII} , assuming that all stars are located at the same position and have a global production rate of Lyman continuum photons N_{Lyc} , equal to the sum of the contribution of the individual stars, and for case B recombination in a diffuse medium of density n_H : $R_{HII} = \left(\frac{3}{4} \frac{N_{Lyc}}{\alpha_B n_H^2}\right)^{1/3}$. In this formula, α_B is the hydrogen recombination coefficient (Osterbrock 1989). The mean radius for R_{HII} is 35 pc .

To constrain the population of massive stars, we calculate different stellar outputs, namely we perform a detailed calculation of the UV radiation field at $912\text{--}2000 \text{ \AA}$, and also compute the global U flux and U radial profile, as well as the thermal radio continuum and H α emission.

• 6 cm radio-continuum.

According to Mezger (1972) and Turner & Ho (1994), the radio continuum emission of HII regions for case B recombination, at an electronic temperature T_e of 10^4 K and with 45 % of the ionizing photons being converted into H α photons, is directly related to N_{Lyc} by:

$$\frac{N_{Lyc}}{s^{-1}} = 1.1 \times 10^{50} \left(\frac{S_{6cm}}{mJy}\right) \left(\frac{D}{Mpc}\right)^2.$$

This formula does not include any correction for dust absorption of the ionizing radiation within the HII region.

Current estimations are that nearly 50% of the Lyman continuum may be absorbed by dust.

• H α .

The relationship between the H α luminosity and the production rate of Lyman continuum photons, using the same assumptions as above, can be deduced from Mezger (1972) and Peimbert et al. (1975):

$$\frac{L_{H\alpha}}{L_{\odot}} = 3.55 \times 10^{-46} \left(\frac{N_{Lyc}}{s^{-1}}\right).$$

The correction for the extinction may amount to about 1 magnitude at H α but it is highly uncertain (Mc Kee & Williams 1997, van der Hulst et al. 1988). Because of the uncertainties involved in this correction, we have preferred not to do it. This allows us to check that the energy is conserved with a good accuracy in the simulation.

The formed OB associations have typical production rates of Lyman continuum photons, N_{Lyc} , in the range $10^{45}\text{--}10^{51} \text{ s}^{-1}$. The cumulative Lyman continuum luminosity function of the population is shown in Fig. 5. Its shape is similar to the distribution for Galactic HII regions (McKee & Williams 1997). There is a small excess around $N_{Lyc} \geq 10^{49.5} \text{ s}^{-1}$, dominated by the most massive stars in the younger associations, and a deficiency of associations with $N_{Lyc} \geq 10^{50.5} \text{ s}^{-1}$. As a whole, the match of the two distributions is very good. The distribution of the intrinsic UV luminosity of OB associations extends over four orders of magnitude from 10^4 to $10^7 L_{\odot}$, i.e. from small associations with about 20 stars and a total stellar mass of $600 M_{\odot}$, up to large associations gathering 200 OB stars, including a few 50-60 M_{\odot} stars, and having a total stellar mass of $6000 M_{\odot}$.

3.4. Dust properties

We use the average Galactic extinction curve from Fitzpatrick & Massa (1988) at UV wavelengths. For visible and near infrared wavelengths, we use the work by Seaton (1979). This curve is probably valid on a large scale in the diffuse medium of NGC 6946 which has a similar metallicity to the Milky Way. We assume a constant metallicity and gas to dust ratio in the disk, and use the average value for the Milky Way : $\frac{NH}{E(B-V)} = 5.8 \times 10^{21} \text{ H cm}^{-2} \text{ mag}^{-1}$ and $A_V = 3.1 E_{B-V}$ (Bohlin et al. 1978). The extinction through a cell filled with molecular gas, with the adopted spatial resolution, is 2.5 magnitudes. The dust properties have been summarized by Bruzual et al. (1988) and Witt & Gordon (1996). Apart from the enhanced absorption in the 2175 \AA bump, the dust albedo is fairly constant at UV and visible wavelengths at $\omega \sim 0.55$. We include the coherent scattering of UV light by dust grains. The anisotropy is described using the Henyey-Greenstein (1941) function, where the anisotropy parameter is defined as $g = \langle \cos \theta \rangle$ and θ is the scattering angle.

3.5. Radiative transfer

The observed properties of external galaxies depend on the propagation of the stellar radiation in the interstellar medium. To determine the local radiation field, we follow the propagation of UV photons (912-2000 Å) emitted from the OB stars in the two phases medium. In each cell, we compute a local radiation field. We define the local radiation field in the UV, χ_{UV} , relative to the mean radiation field in the UV at the Solar radius, χ_0 , established by Mathis et al. (1983), so that $\chi_{UV} = \frac{4\pi J}{\chi_0}$. In the Galaxy and at the solar radius, the InterStellar Radiation Field, ISRF in the UV, has been defined as $\chi_0 = 4\pi J = 4\pi \int_{912\text{\AA}}^{2000\text{\AA}} J_\lambda d\lambda = 1.84 \times 10^{-3} \text{ erg cm}^{-2}\text{s}^{-1}$ and through visible/IR bands as $G_0 = 4\pi \int_{912\text{\AA}}^{2\mu\text{m}} J_\lambda d\lambda = 2 \times 10^{-2} \text{ erg cm}^{-2}\text{s}^{-1}$, where J_λ is the specific intensity of the radiation field averaged over 4π sr (Mathis et al. 1983).

On their path, photons can be scattered and/or absorbed by dust in both neutral phases. We have chosen not to follow individual photons which would have been time consuming, but to use instead pseudo-photons representing a collection of N photons. We are then able to probe a larger area with a lower number of photons. We sample the 912-2000 Å interval with 20 bins of constant wavelength width $\Delta\lambda$, and launch n_γ pseudo-photons per association per wavelength bin. The longward limit has been set to 2000 Å, to avoid having to take into account the contribution from star types later than B to the ISRF (Walterbos & Greenawalt, 1996).

The pseudo-photons emitted by the OB association number i carry a fraction $f_\lambda^i d\lambda$ of the luminosity L_λ^i radiated by this OB association. They travel from the center of a cell (size r_{cell}) to an adjacent one, and the energy absorbed by the interstellar medium, when non-zero, is left on the common face of these 2 cells. The absorbed energy is reprocessed in the far-infrared. The pseudo-photon energy along its path from association number i can be written as :

$$f_\lambda^i d\lambda = \alpha^i \frac{L_\lambda^i}{n_\gamma}$$

In this formula, $\alpha^i = \prod_j \alpha^j(x, y, z)$ is the product of the probabilities for non absorption in each cell along the travel from the OB association number i to the cell position (x, y, z) , or with $\omega(\lambda)$ the dust albedo and τ_λ the total cell opacity including scattering :

$$\alpha^j = e^{-(1-\omega(\lambda))\tau_\lambda}$$

in the diffuse phase, and

$$\alpha^j = \omega(\lambda)$$

in the H₂ phase.

When leaving an OB association, the direction for each pseudo-photon is uniformly chosen on the unit sphere. These pseudo-photons travel in the two-phase interstellar medium. There are different possibilities when reaching a new cell :

- i) The gas in the cell is diffuse and atomic. Then the pseudo-photon can either :
 - be absorbed partially in the cell. A fraction of the luminosity is left, and the pseudo-photon continues in the same direction with a lower luminosity.
 - be scattered.

- ii) The cell is filled with molecular gas.

The pseudo-photon is partly absorbed, and partly backward scattered, the ratio between the energy left in the cell and the total energy of the pseudo-photon depends on the albedo as $1 - \omega(\lambda)$. We have chosen backward scattering in that case to prevent the pseudo-photon from interacting with the same molecular cloud several times.

After a scattering event, a scattering angle θ is chosen according to the anisotropy function, and the azimuthal angle ϕ is uniformly chosen in the interval $[-\pi, \pi]$. Then the new direction is easily deduced from the previous one (Witt 1977).

Since we cannot store all the pseudo-photons' incident directions, and in order to define an isotropic radiation field in each cell, we assume that the equivalent surface of the cell is $6r_{cell}^2$. Then, the UV radiation field in the cell (x, y, z) due to the contributions of all pseudo-photons travelling through this cell, can be expressed relative to the Galactic ISRF χ_0 as :

$$\frac{\chi(x, y, z)}{\chi_0} = \sum_i \sum_{\delta\lambda} \frac{f_\lambda^i d\lambda}{\chi_0 6r_{cell}^2}$$

Because of the coarse angular resolution and the low number of pseudo-photons leaving each OB association, the resultant map of the radiation field presents strong fluctuations. We have chosen to smooth the map of the radiation field by averaging the data in nearby cells, typically 3x3 cells. Furthermore, some cells are never visited by UV photons, for example in the interarm region or in the outer disk ($r \geq 5$ kpc). In that case, we use as incident radiation field, the Galactic ISRF (longward of 2000 Å), scaled by the local surface brightness in the R band image to take into account the radial variation of the radiation field from the old stellar population between the central regions ($r \leq 1$ kpc) and the outer disk ($r \geq 5$ kpc). The reference value is given in units of $4\pi \int_{2000\text{\AA}}^{2\mu\text{m}} J_\lambda d\lambda = G_0$ - $\chi_0 = 1.82 \times 10^{-2} \text{ erg cm}^{-2}\text{s}^{-1}$. The position for the reference value has been chosen at the edge of a spiral arm, at a distance $r = 4$ kpc from the center, where the UV radiation field χ_{UV} is close to 1.

3.6. Emergent emission.

Once the local UV energy density has been calculated, models are used to determine the C⁺ and FIR emissions from each cell, assuming that they arise from the same area as the one used for the calculation of the UV radiation field. For the dust emission, we use the model by Désert et al. (1990), which has 3 different components: PAHs which

are fully ionized when $\chi_{UV} > 1$, very small grains and big grains. We calculate the dust emission in the four IRAS bands at 12, 25, 60 and 100 μm plus an additional band at 200 μm , as the reprocessing of the combination of the UV radiation field (912 - 2000 Å) described by χ_{UV} and of the ISRF for the 2000 Å-2 μm part of the spectrum. We decrease the PAH abundance in large radiation field environments, as suggested by Ryter et al. (1987), to one fifth of the standard value when $\chi_{UV} > 100$.

Very large molecular clouds, with masses larger than $10^6 M_\odot$ occupy more than 4 cells in the grid. The inner cell is not directly exposed to the UV radiation and for this cell we assume that the ISRF is attenuated by 2.5 magnitudes of visual extinction.

We assume low optical depth in the mid and far infrared. From the analysis of the COBE maps of the Galaxy, Boulanger et al. (1996) deduce $\tau_\lambda/N_H = 1 \times 10^{-25} \text{ cm}^2 \text{ H}^{-1} (\lambda / 250 \mu\text{m})^{-2}$, which combined with the mean column density of individual clouds, $N_H = 1.5 \times 10^{22} \text{ cm}^{-2}$, gives an opacity of 2×10^{-3} at 200 μm .

According to the dominant phase in a given cell of the model, the emergent infrared emission can be :

- reprocessing of the whole incident stellar radiation for molecular clouds which are totally optically thick in the UV. All impinging radiation is completely reprocessed in infrared emission from the outer cells of molecular clouds,
- proportional to the gas column density for the diffuse medium, which is optically thin in the UV. We assume no UV extinction at the 12 pc scale.

We use the PhotoDissociation Region (PDR) model by Le Bourlot et al. (1993) to estimate the $^2P_{3/2} - ^2P_{1/2}$ C⁺ emission at the surfaces of molecular clouds. We use a constant molecular hydrogen density of $5 \times 10^3 \text{ H}_2 \text{ cm}^{-3}$ and the incident UV field χ_{UV} . The density is not a critical parameter as long as it is higher than the critical density for collisional excitation of C⁺ (1000 H cm^{-3}) (see Tielens & Hollenbach 1985). Furthermore, we assume that the whole surface of clouds contributes to the C⁺ emission. As for the C⁺ emission from the diffuse neutral phase, we use the model by Wolfire et al. (1995) for a two phase neutral atomic medium. Finally, the contribution from the ionized gas in the HII regions around the OB associations is also included. We assume that the gas has the same density as the diffuse medium, $n_e = n_H$ and an electronic temperature of 10^4 K . The total C⁺ luminosity from an HII region of radius R_0 is then proportional to the volume of the HII region with a correction factor to take into account the other ionization stages of carbon.

Because we deal with a line, the opacity may not be small depending on the gas distribution and viewing geometry. In fact, opacity effects are important at large inclination angles. To obtain an edge-on view of the model galaxy in the $^2P_{3/2} - ^2P_{1/2}$ C⁺ line, we have made an accurate calculation of the radiative transfer in this line. For each line of sight through the disk, we sample the line profile with bins of 1 kms^{-1} width, and calculate the emergent

intensity in each velocity bin, including saturation effects. We assume that the intrinsic velocity dispersion of a PDR is 1 kms^{-1} . For the diffuse medium, the velocity dispersion is 10 kms^{-1} . We do not account for absorption in the far infrared continuum. We obtain $\tau_{C^+} = 0.40$ for an edge-on view, and $\tau_{C^+} = 0.10$ for a face-on view.

3.7. Implementation of the model

To avoid transient stages of the simulation, the code is evolved during a few time steps. We stop the simulation when stable results are obtained on a time scale of 20 Myrs. This time scale corresponds to about half the lifetime of a giant molecular cloud before disruption by photoevaporation. This is the reason why we can not integrate further in time without treating gas recycling. The time step has been fixed at 10^6 years, shorter than the lifetime of the most massive stars. We have checked the reliability of the calculations by different tests:

- We have verified that the total UV luminosity from the stellar population emerges from the galaxy either at the same wavelength, or at far infrared wavelengths for the light reprocessed by dust grains. The total luminosity is conserved with an accuracy of 1 %.
- When the number of pseudo-photons leaving each OB association n_γ is too small, the map of UV radiation field is noisy with a few extremely bright spots and large voids. This is due to undersampling of the galaxy volume. The number of pseudo-photons should be as large as possible, but we have verified that we obtain a good map of the UV radiation field with 100 pseudo-photons per OB association. The map is smooth in the vicinity of the OB associations, hence the ratio of FIR emissions from the diffuse and dense gas stays constant with increasing n_γ .
- The cell size is also a critical parameter: since χ_{UV} is proportional to r_{cell}^{-2} , it might be underestimated for small clouds very close to OB associations. This has severe consequences for the C⁺ emission, which scales roughly as $r_{cell}^2 \log(\chi_{UV})$, but little or none for the FIR emission which varies as $r_{cell}^2 \chi_{UV}$ since in that case there is no resultant scaling with r_{cell} . To test the validity of the adopted resolution, we have performed a run restricted to one quadrant only, with a cell size of 6.1 pc. We observed no large variation in the C⁺ emission and thus conclude that the adopted resolution of 12 pc is correct for our purpose. Note that the volume filling factor decreases to 1.3 % in the high resolution run, because we fill the space in a more accurate way using a higher spatial resolution.

4. Results

Table 2 summarizes the input parameters for the Standard Model, and Table 3 presents the results. The star formation rate from 2 to 60 M_\odot is fixed at $4.0 M_\odot \text{ yr}^{-1}$, with a star formation efficiency ϵ of 5%, as defined in Sect. 3.4. With these values, the modelled H α luminosity and

H α radial profile are in quite good agreement with the observed data (Kennicutt 1989). This is also true for the UV luminosity at 2000 Å and the 6 cm luminosity. We are thus confident that the massive star population is well constrained by the observed data. With a low mass cut-off at 10 M $_{\odot}$ stars, we overestimate the UV luminosity at 2000 Å of the modelled stellar population by 20%, because we miss the contribution to the UV continuum of lower mass stars, between 2 and 10 M $_{\odot}$.

4.1. Disk opacity in the UV

We have computed an average opacity over the galaxy in the UV and for the H α line. We define this opacity as : $\tau = -\ln(L^{emergent}/L^{emitted})$ where $L^{emitted}$ is the total luminosity in the disk at a given wavelength and $L^{emergent}$ is the emergent luminosity. This opacity is computed for two different viewing angles of the model, $i = 0^\circ$ for face-on and $i = 90^\circ$ for edge-on. We have found a significant opacity for the face-on view, at 1000 Å, 2000 Å and for H α , namely $\tau(1000\text{Å}) = 0.8$, $\tau(2000\text{Å}) = 0.7$, $\tau(H\alpha) = 0.60$ for the whole galaxy.

The opacity is controlled simultaneously by the geometry of the molecular cloud ensemble and by the diffuse medium. If we ignore the extinction due to the diffuse component, we find an opacity of 0.51 at 1000 Å. This value is due to geometrical effects, mostly blocking of the UV radiation by molecular clouds, and it does not depend on wavelength. Thus we can write the opacity at any wavelength in the UV as $\tau_\lambda = 0.51 + \tau_\lambda^{HI}$, the second term accounting for the wavelength dependence of the extinction in the diffuse medium.

A global opacity of $\tau \simeq 0.8$ corresponds to a fraction of approximatively 45% of the far UV stellar radiation leaving the galaxy disk, mostly above or below the main plane. Most of these photons have not been scattered because the probability of leaving the disc after a scattering event is low. This significant fraction of the radiation from massive stars leaking out of HII regions could contribute to the maintenance of the Reynolds layer of ionized gas. The derived face-on opacity at 2000 Å, 0.7, falls well within the range of opacities derived by Buat & Xu (1996). The mean extinction in their sample of nearby spiral galaxies is $\simeq 0.9$ mag at 2000 Å. Though the opacity is not very large, the mean distance travelled by a UV photon before absorption is quite small, 440 pc, roughly equal to the HI disc thickness. As shown on Fig. 6, there are however photons travelling to much larger distances, 1 to 2 kpc, with a small probability (0.01). Conversely, many zones in the interarm receive very few UV photons. Due to the lower gas density, few OB associations are created in the interarm region. The numerous OB associations in the arms are too distant to contribute to the local radiation field since the arm/interarm separation is larger than 1 kpc in the disk.

The distribution of χ_{UV} values provide further information on the radiation field resulting from the OB associations (Fig. 7). Whereas most of the galaxy is exposed to a low UV radiation field, it is possible to find regions with high UV intensity ($\chi_{UV} \geq 1000$) even at a moderate spatial resolution. The total dynamical range of the UV radiation field extends over more than 4 orders of magnitude. This huge variation can be explained by the close association of OB associations and molecular clouds: in a galaxy with a prominent spiral structure, OB associations are born in the spiral arms, where the gas density is the highest. This maximizes both the illumination of molecular clouds by UV radiation and the absorption of UV radiation by molecular gas, hence the heating of molecular gas. For the model galaxy, we find that 30 % of the total number of cells with molecular gas are exposed to a strong or median radiation field ($\chi_{UV} \geq 10$). These cells are located in 40% of the molecular clouds. This figure is comparable to the clouds in Milky Way: Solomon et al. (1985) found that in the Galaxy, at a resolution greater than 10 pc, 25 % of the molecular clouds are warm and associated with HII regions. Also, Williams and McKee (1997) estimate that at least one OB star is present in half of the giant molecular clouds with masses larger than 10^5 M $_{\odot}$. The probability to find massive stars or clusters associated with a giant molecular cloud increases sharply with the cloud mass and reaches almost 1 for masses larger than 8×10^5 M $_{\odot}$ (Williams & MacKee 1997). Our numerical results are in agreement with these facts.

4.2. Far infrared emission

We now discuss the emergent radiation from the model galaxy and start with the infrared emission. As in the Désert et al. (1990) dust model, the luminosities in the IRAS bands are computed as $4\pi D^2 \nu S_\nu$, where S_ν is the total observed flux density and D is the distance to the object. The infrared colors are given as the flux density ratios, to compare with observed data.

The model galaxy has very similar emissions as NGC 6946 at 60-100 & 200 μm , with outputs of 5.1, 8.5 and 4.9×10^9 L $_{\odot}$, corresponding to 114%, 128% and 144% of the luminosities observed at those wavelengths. The far infrared emission comes from both the molecular and atomic gas phases.

The UV radiation is the main heating mechanism of the dense and diffuse gas phases, with contributions of 4.2×10^9 L $_{\odot}$ and 6.1×10^9 L $_{\odot}$ at 60 & 100 μm . The contribution to the FIR emission of the old stellar population, described by the ISRF, is a factor 3 lower, with 0.9×10^9 L $_{\odot}$ and 2.4×10^9 L $_{\odot}$ in the 60 & 100 μm bands. The situation is different at 200 μm , where dust grains heated by the UV radiation or by the ISRF have almost equal contributions to the total luminosity: 3.0×10^9 L $_{\odot}$ for the UV and 1.9×10^9 L $_{\odot}$ for the ISRF. The contribution from the inner parts of clouds illuminated by the attenuated ISRF

is only $0.5 \times 10^8 L_{\odot}$. As a whole, 72 % of the far infrared luminosity can be attributed to UV heated gas, which is mostly molecular. The remaining 28% corresponds to dust heated by the ISRF, at locations far away from the OB associations.

The diffuse and dense phases have similar contributions to the total FIR emission, with a slight excess from the molecular clouds, 54 % versus 46 % from the diffuse gas. This significant contribution from the diffuse gas is due to the fact that it occupies a large fraction of the galaxy volume. Hippelein et al. (1996) also conclude from ISO observations of other nearby galaxies (M51, M101) that the neutral atomic gas has an important contribution to the far infrared emission. The contribution from the atomic gas may be underestimated because we do not take into account the compression of the diffuse gas in the spiral structure. Comparing with molecular clouds, we can estimate that, having atomic gas concentrated in the spiral arms would result in a brighter FIR emission, with a slightly warmer color temperature since the dust grains would be closer (in average) to the heating sources. A precise estimate of the magnitude of the effect is beyond the scope of this paper.

The global infrared excess for the model galaxy, IRE, is defined as the luminosity ratio $IRE = L_{12-100\mu m} / L_{Ly}$, with $L_{Ly} = N_{Ly} h\nu_{Ly}$ and $h\nu_{Ly} = 13.6$ eV. At the disk scale, the IRE takes the value 5.9, in agreement with observations of Galactic HII regions (Caux et al. 1985, Myers et al. 1986).

The diffuse and dense gas (atomic and molecular) have the following contributions to the total luminosity of the C⁺ 158 μm line: 77% from the dense phase and 23% from the diffuse phase. Less than $10^4 L_{\odot}$ comes from HII regions. The total emission of the galaxy is $2.5 \times 10^7 L_{\odot}$, a factor 2.5 lower than the measured value, $6.3 \times 10^7 L_{\odot}$ (Madden et al. 1993). Compared to the 60-100 μm far infrared emission, the C⁺ line represents 0.21% of the FIR (60-100 μm) emission. This figure is comparable to the observed ratio for other spiral galaxies with 0.1 - 1 % (Lord et al. 1996). Nevertheless, the value for NGC 6946 was found to be 0.6 % (Madden et al. 1993), and in the Galaxy, Shibai et al. (1991) and Wright et al. (1991) have measured $L_{C^+} = 0.7 \% L_{FIR}$ with the same definition of L_{FIR} as above.

4.3. Radial profiles

The 60 μm radial profile is shown on Fig. 8a. There is a large decrease from the inner to the outer parts of the disk, about two orders of magnitude. In NGC 6946, the same behaviour has been observed by Tuffs et al. (1996) using ISO. Averaged over the model, the S_{60}/S_{100} infrared color appears to be slightly different in the two phases: 0.32 for the diffuse phase and 0.38 for the dense phase. This FIR color decreases with increasing radius from 0.40 in

the center to 0.23 at $R \simeq 5$ kpc (Fig 8b), in agreement with the maps by Engargiola (1991). The decrease is seen in both phases, with S_{60}/S_{100} ranging from 0.35 to 0.23 for the diffuse phase, and from 0.42 to 0.28 for the dense phase.

The radial profile of the intensity of the C⁺ $^2P_{3/2} - ^2P_{1/2}$ 158 μm line (Fig. 8c) shows a much flatter gradient than the FIR emission. This is due to the logarithmic dependence of the line intensity on the incident radiation field in PDRs. As shown in Fig. 8c and 8d, the diffuse atomic gas is the main source of C⁺ emission at large distance from the nucleus, for radii larger than 4 kpc. It is thus possible to determine the intrinsic L_{C^+}/L_{FIR} luminosity ratio from the two gas phases, using the data at $R \sim 2$ kpc for the molecular gas and data at $R \geq 5$ kpc for the atomic gas. We find that L_{C^+}/L_{FIR} is equal to 0.10 % in the diffuse phase and to 0.25% in the dense phase.

4.4. Maps

We show on Fig. 9 face-on maps of 100 μm , C⁺ and UV(912-2000 Å) emissions. Edge-on maps at the same wavelengths are shown in Fig. 10 for comparison. Compared to the C⁺ observations of the edge-on galaxy NGC 891 (Madden et al. 1994), there is an overall agreement. In particular, the scale height in C⁺ is predicted to be larger than the scale height of the CO emission, due to the contribution of the diffuse neutral and ionized media which have a larger scale height (Fig. 11).

In the face-on C⁺ map, there is a large hole in the inter-arm regions in the NW, at a similar position to the hole detected by Madden et al. (1993) with the KAO. This hole is due to the lower density of molecular gas and of OB associations in the interarm regions. Therefore few UV photons illuminate this region and the radiation field is very low. The map shows many details and a large contrast between arm and interarm regions. We have smoothed the image from the model to the resolution of the KAO observations (50" beam = 1.2 kpc at the distance of NGC 6946). The contrast between the brightest regions and the disk drops by a large factor. This resolution effect may explain the low dynamical range found in the observed data. If PDRs are the main source of C⁺ 158 μm radiation in galaxies, we predict that the emission should have more contrast at higher spatial resolution. This could be tested by maps of external galaxies made with the future Stratospheric Observatory For Infrared Astronomy (SOFIA).

The edge-on maps at 100 μm and in C⁺ are fairly symmetrical with respect to the center. The edge-on C⁺ map shows however a hole in the central region ($r < 500$ pc) which does not appear on the 100 μm map. This hole is largely due to the large opacity for these lines of sight ($\tau_{C^+} = 0.4$).

4.5. Sensitivity of the model to input parameters

The model results are of course sensitive to the input parameters, therefore we have run different models deviating from the standard model by one parameter.

Because of the poor knowledge of the albedo in UV, we have run a model with a lower albedo of dust grains, $\omega = 0.4$. We find that the opacity increases to 1.0 at 1000 Å & 0.90 at 2000 Å. The 60 μm emission from the dense phase increases by 5%, while the 100 and 200 μm emissions both decrease by 10%. This difference in far infrared emission is due to the moderate increase of the opacity which leads to a warmer dust temperature. The effect on the emission from the diffuse phase is negligible.

A more extreme case is for a null albedo, suppressing any scattering effect. In that case, we maximize the UV opacity and the FIR emission. The opacity increases to 1.25 at 1000 Å and 1.01 at 2000 Å respectively. As a result of this larger absorption, the 60-200 μm emission increases by 47 % as compared to the standard model.

In another run, we have kept the total mass of molecular gas constant, but used a lower mean density, 20 $\text{H}_2 \text{ cm}^{-3}$ instead of 50 $\text{H}_2 \text{ cm}^{-3}$, to increase the clouds sizes. The volume filling factor is then 3.8 %. These larger clouds block more light, and 30 % only of the molecular cells are heated, instead of 40% in the standard model. As a result, the 60-200 μm luminosity decreases by 10%, to $16.7 \times 10^9 L_\odot$.

We have also investigated the effect of the number of OB associations: we have kept the same star formation rate but have gathered adjacent associations to form more powerful sources. As a consequence, n_{OB} decreases from 12000 to 3000. Then a smaller fraction of the cloud population is heated, 15%, as compared to 40% in the standard model. But because these cells are heated by more powerful OB associations, the far-infrared emission is larger and reaches $20.4 \times 10^9 L_\odot$. Thus the FIR emission depends slightly on the number of associations. The C⁺ emission decreases to $1.8 \times 10^7 L_\odot$, because of the smaller number of illuminated clouds.

If we now increase the SF efficiency, from 5 to 10%, so as to double the UV luminosity, the production rate of Lyman continuum photons increases by 80 %. In that case, the mean UV opacity is 0.78. The FIR 60-200 μm luminosity increases by 55 % to $28.7 \times 10^9 L_\odot$. This shows that the FIR emission is not a linear function of the UV luminosity in our model. This non-linear behaviour arises because the opacity is largely controlled by geometrical effects. With a larger star formation activity, HII regions are very large and can destroy molecular clouds efficiently. Thus the mass of molecular gas decreases in the model with a higher SFR. This is the main reason for the non-linear behaviour. This result has been established with the same number of OB associations, while an increased SFR will probably lead to more associations in the disk. How-

ever we have previously shown that the FIR emission does not depend strongly on the number of OB associations.

We have investigated the effect of the atomic density on the size of HII regions, because we probably overestimate the diameter of HII regions, using a mean atomic density and neglecting the dust absorption. If the local gas density is multiplied by two, the volume of the Strömgren sphere is 4 times smaller than in the standard model. The 60-200 μm luminosity of dense molecular gas increases by 10% to $1.1 \times 10^{10} L_\odot$. This is explained by the reduced destructive effect of HII regions on molecular clouds, and then the larger chance for photons to be absorbed by molecular gas. The respective contributions from the diffuse and dense gas to the FIR(60-200 μm) are now 34% and 66%.

This last test shows that the distance between clouds and OB associations has a strong influence on the UV reprocessing by dense gas. For the standard model, we have calculated the mean distance between an OB association and the nearest cloud edge, $d_{OB/cloud}$, and have found a value of 35 pc, the mean distance between clouds centers is 37 pc. To have a larger separation between clouds and OB associations, we have increased v_{escape} to 30 kms^{-1} . We obtain $d_{OB/cloud} = 39$ pc. The FIR(60-200 μm) emission from the dense phase decreases by 15% because of the smaller solid angles of the clouds viewed from the associations. As for the FIR (60-200 μm) from the diffuse phase, it slightly increases by 6%.

We have shown that part of the UV opacity is due to geometrical effects. Indeed the UV opacity is lower when the molecular clouds are distributed uniformly in the disk. We have used an earlier epoch of the simulation, when the distribution of gas clouds is axisymmetric. We have kept the same value for the other parameters (number of OB associations, star formation rate, etc.). In that case, the clouds occupy a larger fraction volume of the galactic disk, and the mean distance between clouds increases. Because of this larger mean distance between clouds, the opacity at 1000 Å decreases to 0.47.

5. Discussion & conclusions

We have shown that with simple assumptions about the birth of massive stars and their relationships with the ISM, we can reproduce qualitatively and quantitatively the characteristics of the UV, H α and FIR emissions of a particular object, the Sc galaxy NGC 6946. For such a galaxy with a prominent spiral structure, having a large mass of neutral gas, and forming stars actively, the observed far infrared emission is produced both in molecular gas and in the diffuse atomic gas. More precisely, 54 % of the FIR (60-200 μm) emission comes from dust grains in giant molecular clouds. Dust in the diffuse neutral atomic gas contributes to about 46 % of the total FIR luminosity.

We have evaluated the respective contributions of the UV radiation from massive stars and of the radiation field

from the old stellar population. We find that 72 % of the FIR luminosity can be attributed to UV heated dust grains, which reside mostly in molecular clouds envelopes. The remaining 28 % is due to dust heated by the radiation field from the old stellar population at locations far away from OB associations.

We have calculated the emission of the model galaxy in the $^2P_{3/2} - ^2P_{1/2}$ fine structure line of C⁺ at 158 μm . In the spiral arms, photon dissociation regions at the surfaces of molecular clouds are the main source of the emission. We have found a large arm-interarm contrast in this line. This effect could be tested by high angular resolution maps of galaxies. It results naturally from the combination of a lower gas density and lower radiation field in the interarm regions, because of the short mean free path for UV photons, ~ 440 pc. As a whole, PDRs represent 76% of the emission. The contribution from the diffuse phase is found to be ~ 24 %. Our model is able to account for about 40 % of the observed C⁺ emission of NGC 6946. The emission from PDRs should be viewed as a lower limit since we use the model by Le Boulot et al. (1993) with low abundances of carbon and other elements in the gas phase: $[\text{C}]/[\text{H}] = 3 \times 10^{-5}$. The average value is 1.3×10^{-4} for Galactic diffuse clouds (Snow & Witt 1996), a factor of 4 larger than the value used in the model. Since the C⁺ 158 μm emission scales roughly with the column density, hence the carbon abundance, the total C⁺ luminosity from PDRs could be larger by at least a factor three than our current model prediction. This would increase the contribution from PDRs to the total C⁺ emission of the model galaxy: with this scaling factor, the predicted C⁺ luminosity of PDRs would reach $6 \times 10^7 L_{\odot}$. Moreover, the C⁺ emission from the diffuse gas is overestimated, because the model of Wolfire et al. (1995) assumes $[\text{C}]/[\text{H}] \sim 3 \times 10^{-4}$ in the gas. Thus the diffuse emission could be 2-3 times smaller than in our standard model. Adopting $[\text{C}]/[\text{H}] = 1.3 \times 10^{-4}$ in both phases would thus enhance the differences of $L_{\text{C}^+}/L_{\text{FIR}}$ between dense and diffuse gas.

The knowledge of the cloudy nature of the ISM, and of the global structure of the galaxy, is important to determine how far UV photons can travel away from OB associations. The filling factor and the mass/radius scaling law appear to be major parameters for the transfer of stellar radiation in the galaxy disk, because they determine at the same time the obscuration and the size of the emitting regions. Other important parameters are the number of OB associations and the sizes of HII regions, because with a large number of OB associations or with small HII regions, molecular clouds are on average closer to massive stars, and are thus more efficiently heated.

In all the models we ran, we have found that the average internal UV opacity is of the order 0.8. The discs are therefore moderately opaque in the UV, as measured by Buat & Xu (1996). This moderate opacity holds for face-on discs. Edge-on discs are quite opaque, with a small fraction of the luminosity escaping, less than 1.0% of the

face-on luminosity. This fraction corresponds to an equivalent extinction of 5 magnitudes in the UV.

These results have been obtained using a crude description of the interstellar medium. The adopted spatial resolution results from a compromise between astrophysical requirements and computational needs, but is certainly very poor compared to the complexity of the interstellar medium. The good agreement of the observed and predicted large scale properties shows nevertheless that the transfer of UV radiation, and the role of the radiation for the gas and dust heating, are correctly described at the 12 pc scale. This is in agreement with previous works estimating that dust heating by UV radiation occurs principally at large distances from massive stars (Murthy et al. 1992, Leisawitz & Hauser 1988).

Acknowledgements. We have benefited from the help of F. Viallefond for the numerical calculations and the data processing, and from discussions with D. Beck, G. Helou, S. Madden, S. Shore. We thank F.X. Désert and J. Le Boulot for letting us use their codes, and M.G. Wolfire for providing unpublished results.

—

Figure captions

Fig. 1. CO(J=2-1) map at 13'' resolution obtained with the IRAM 30m radiotelescope.

Fig. 2. V-I image, obtained with the 1.20m telescope at the Observatoire de Haute Provence (P. Boissé, private communication). The field of view is 10' by 10', the pixel size is 2.3''. The gray scale runs from white for blue colors to black is for red colors.

Fig. 3a. R band image of NGC 6946 used as input for the calculation of the gravitational potential. Field stars have been removed, the image has then been rotated and de-projected to get a face-on view of NGC 6946.

Fig. 3b. A face-on view of the model galaxy, with molecular clouds drawn as circles and OB associations drawn as stars. Only 20 % of the OB associations and molecular clouds are drawn.

Fig. 3c. A close-up view of Fig. 3b. The clouds are drawn at their exact size in the model.

Fig. 4. Adopted rotation curve (dot-dashed line), angular frequency $\Omega(r)$ (full line), and $\Omega \pm \frac{\kappa}{2}$ curves. The corotation for the adopted pattern speed is located at $r = 3.5$ kpc.

Fig. 5. Distribution of the production rate of Lyman continuum photons N_{Lyc} , for the modelled population of OB associations (full line) in NGC 6946, and for the Galaxy (dot-dashed curve) (McKee & Williams (1997)). The plot can be read for instance as 500 OB associations out of 12000 have $N_{Lyc} > 10^{50} \text{ s}^{-1}$.

Fig. 6. Distribution of the distance from their parent OB association, travelled by UV photons before absorption. The median distance is 120 pc, and the mean distance is 440 pc.

Fig. 7. Distribution of the UV intensity measured relative to the ISRF in the modelled galaxy, for cells filled with diffuse gas (dot-dashed line) and for cells filled with molecular gas (full line).

Fig. 8a. Radial profiles of the 60 μm surface brightness. The thin solid line shows the combination of the two gas phases, while the triangles show the contribution of the diffuse atomic gas, and the squares the contribution from the molecular gas. The thick solid line shows the mean radial profile deduced by Engargiola (1991) from an IRAS image.

Fig. 8b. Radial profiles for the ratio of 60 and 100 μm fluxes, global and for the two phases.

Fig. 8c. Radial profiles of the C⁺ emission: global and for the two phases.

Fig. 8d. Radial profiles of $L_C^+ / L_{(60-100\mu\text{m})}$: global and for the two phases.

Fig. 9. Face-on views of:

a) 100 μm emission, at 48 pc resolution. The gray scale ranges from 1 to $10^3 \text{ L}_\odot \text{ pc}^{-2}$. We have overlaid contours of the same map convolved with a 750 pc beam: the levels are at 10, 30, 60, 100, 200 $\text{L}_\odot \text{ pc}^{-2}$.

b) C⁺ line, at 48 pc resolution. The gray scale ranges from

10^{-2} to $1 \text{ L}_\odot \text{ pc}^{-2}$. Overlaid contour levels from 0.1 to 0.6 by $0.1 \text{ L}_\odot \text{ pc}^{-2}$ for the same image convolved with a 750 pc beam.

c) emergent UV surface brightness (resolution: 48 pc). The gray scale ranges from 10^{-2} to $10^5 \text{ L}_\odot \text{ pc}^{-2}$.

Fig. 10. Edge-on views of NGC 6946, at 48 pc resolution. The linear scale is not identical for both axes.

a) 100 μm IRAS band, with contour levels at 10^3 , 3×10^3 , 6×10^3 and $10^4 \text{ L}_\odot \text{ pc}^{-2}$.

b) C⁺, at the same resolution, accounting for the line opacity. The gray scale ranges from 0 to $50 \text{ L}_\odot \text{ pc}^{-2}$. Contour levels from 10 to 50 by $10 \text{ L}_\odot \text{ pc}^{-2}$.

Fig. 11. Average vertical profiles through the disk for the C⁺ (dot-dashed line) and CO(1-0)(full line) emissions. The CO(1-0) profile presents a smaller scaleheight (40 pc) than the C⁺ profile (100 pc). We have assumed that the CO(1-0) emission is proportional to the molecular gas column density.

Table 1. Observed parameters for NGC 6946.

Observed data	Value	Reference
Distance	5 Mpc	De Vaucouleurs (1979)
Inclination	34°	Considère & Athanassoula (1988)
M_{H_2} ($R < 6'$)	$2.0 \cdot 10^9 M_\odot$ ¹	Young & Scoville (1982)
M_{HI} ($R < 6'$)	$2.6 \cdot 10^9 M_\odot$ ²	Boulanger & Viallefond (1992)
$L_{1950-2050A}$	$5.4 \cdot 10^8 L_\odot$ ³	Buat et al. (1989)
$L_{H\alpha}$	$1.0 \cdot 10^8 L_\odot$ ⁴	DeGioia et al. (1984))
B_I^0	8.49 mag	RC3
IRAS 12 μ m	$2.3 \cdot 10^9 L_\odot \pm 20\%$ ⁵	Engargiola (1991)
IRAS 25 μ m	$1.4 \cdot 10^9 L_\odot \pm 20\%$ ⁵	Engargiola (1991)
IRAS 60 μ m	$4.5 \cdot 10^9 L_\odot \pm 20\%$ ⁵	Engargiola (1991)
IRAS 100 μ m	$6.6 \cdot 10^9 L_\odot \pm 20\%$ ⁵	Engargiola (1991)
IRAS 200 μ m	$3.4 \cdot 10^9 L_\odot \pm 20\%$ ⁵	Engargiola (1991)
L_{C^+}	$6.3 \cdot 10^7 L_\odot$ ⁶	Madden et al. (1993)
$S_{6cm}^{thermal}$	83 mJy $\pm 25\%$ ⁷	Klein et al. (1982)

We use the value 3.8×10^{33} erg s⁻¹ for the solar luminosity at any wavelength.

¹ We use $N_{H_2}/I_{CO(1-0)} = 2.3 \cdot 10^{20}$ mol cm⁻²/(K kms⁻¹) and a total intensity $I_{CO(1-0)} = 569$ Kkms⁻¹ in a 45" beam, we do not account for projection effects.

² We use $M_{HI} = 1.9 \times 10^{10} M_\odot$ at a distance of 10 Mpc, corresponding to $4.7 \times 10^9 M_\odot$ for a distance of 5 Mpc. By performing an integration over the HI map, we estimate that the part with $R < 6'$ contributes to 55 % of the global emission.

³ The 2000 Å flux, 6.92×10^{-12} erg cm⁻²s⁻¹Å⁻¹, is corrected for the Galactic extinction and integrated over a 100 Å band. Note that Donas & Deharveng (1987) have reported a flux at 2000 Å twenty times lower (1.66×10^{-13} erg cm⁻²s⁻¹Å⁻¹). Measurements at other UV wavelengths are available in Rifatto et al. (1995).

⁴ We use the uncorrected flux $f_{H\alpha} = 1.31 \times 10^{-10}$ erg cm⁻²s⁻¹ and the relationship $L_{H\alpha} = 3.13 \times 10^{16} D_{Mpc}^2 f_{H\alpha}$ from Young et al. (1996). We have subtracted the contribution from the nucleus, estimated to be 20 % of the total luminosity. Note that Young et al. (1996) give a lower total flux, 3.38×10^{-11} erg cm⁻²s⁻¹, while Kennicutt (1989) reports a mean surface brightness of 4.2×10^{32} erg s⁻¹ pc⁻² corresponding to a total H α luminosity of $3 \times 10^7 L_\odot$ at the adopted distance.

⁵ We estimate the luminosity in the band centered on frequency ν , by νF_ν . We use the IRAS and KAO fluxes reported by Engargiola (1991) for a radius $R < 5.6'$ and correct from the contribution of the nucleus (central 45") to obtain 12 Jy at 12 μ m, 15 Jy at 25 μ m, 114 Jy at 60 μ m, 283 Jy at 100 μ m and 288 Jy at 200 μ m. The global color for the disk is $S_{60}/S_{100} = 0.40$. The far infrared luminosity is $L_{FIR(60-100\mu m)} = L_{60\mu} + L_{100\mu} = 1.1 \times 10^{10} L_\odot$, $L_{FIR(60-200\mu m)} = 1.45 \times 10^{10} L_\odot$.

⁶ We have excluded the contribution of the nucleus and rescaled the data by Madden et al. (1993) for the adopted distance.

⁷ We use an estimation of 625 mJy for the total flux at 6cm (Klein et al. 1982), subtract the nuclear contribution estimated to be 33% of the total flux, and we keep 20% of the resultant disk flux as the thermal component.

Table 2. Input parameters for the standard model.

Parameter	Adopted value
cell resolution	12.2 pc
HI half thickness	180 pc
H ₂ scaleheight	65 pc
mean V_{OB}	10 kms ⁻¹
n_γ	100
time step	10 ⁶ years
number of molecular clouds	18000
number of OB associations	12000
star formation rate (2 – 60 M _⊙)	4.0 M _⊙ yr ⁻¹
volume filling factor of H ₂	2.5 %

Table 3. Output values from the simulation for the standard model.

Parameter	Total	Dense	Diffuse	UV	ISRF
L _{912–2000 Å} (L _⊙)	1.3 10 ¹⁰	—	—	—	—
L _{1950–2050 Å} (L _⊙)	5.2 10 ⁸	—	—	—	—
L _{Hα} (L _⊙)	1.2 10 ⁸	—	—	—	—
B _t ⁰ (mag)	8.96	—	—	—	—
L ₁₂ (L _⊙)	2.1 10 ⁹	1.0 10 ⁹	1.0 10 ⁹	1.7 10 ⁹	0.3 10 ⁹
L ₂₅ (L _⊙)	2.0 10 ⁹	1.0 10 ⁹	1.0 10 ⁹	1.7 10 ⁹	0.3 10 ⁹
L ₆₀ (L _⊙)	5.1 10 ⁹	2.9 10 ⁹	2.2 10 ⁹	4.2 10 ⁹	0.9 10 ⁹
L ₁₀₀ (L _⊙)	8.5 10 ⁹	4.5 10 ⁹	4.0 10 ⁹	6.1 10 ⁹	2.4 10 ⁹
L ₂₀₀ (L _⊙)	4.9 10 ⁹	2.5 10 ⁹	2.5 10 ⁹	3.0 10 ⁹	1.9 10 ⁹
L _{60–200} (L _⊙)	18.6 10 ⁹	9.9 10 ⁹	8.6 10 ⁹	13.3 10 ⁹	5.2 10 ⁹
L _{C+} (L _⊙)	2.6 10 ⁷	2.0 10 ⁷	0.6 10 ⁷	—	—
S _{6cm} (mJy)	124	—	—	—	—
L _{C+} /L _{FIR} (60–100)	0.18 %	0.25 %	0.10 %	—	—

All luminosities are emergent luminosities. The total UV luminosity generated by OB associations in the disk between 912 and 2000 Å is 3.10×10^{10} L_⊙.

References

- Bohlin R.C., Savage B.D., Drake J.F., 1978, ApJ 224, 132
 Bonnarel F., Boulesteix J., Georgelin Y.P. et al., 1988, A&A 189, 59
 Boulanger F., Viallefond F., 1992, A&A 266, 37
 Boulanger F., Abergel A., Bernard J.P. et al., 1996, A&A 312, 256
 Bruzual A.G., Magris G., Calvet N., 1988, ApJ 333, 673
 Buat V., Xu C., 1996, A&A 306, 61
 Buat V., Deharveng J.M., Donas J., 1989, A&A 223, 42
 Calzetti D., Kinney A.L., Storchi-Bergman T., 1995, ApJ 429, 582
 Casoli F., Clausset F., Viallefond F., Combes F., Boulanger F., 1990, A&A 233, 357
 Caux E., Puget J.L., Serra G., Gispert R., Ryter C., 1985, A&A 144, 37
 Clausset F., Casoli F., Viallefond F., Combes F., 1991, in *Dynamics of galaxies and their molecular cloud distribution*, F. Combes, F. Casoli eds, p. 88
 Combes F., Gerin M., 1985, A&A 150, 327
 Considère S., Athanassoula E. 1988, A&AS 76, 365
 Cox P., Mezger P.G., 1989, A&AR 1, 49
 Cox P., Krügel E., Mezger P.G., 1986, A&A 155, 380
 DeGioa-Eastwood K., et al., 1984, ApJ 278, 564
 Désert F.X., Boulanger F., Puget J.L., 1990, A&A 237, 215
 Devereux N.A., Young J., 1990, ApJ 350, L25
 de Vaucouleurs G., 1979, ApJ 227, 380
 Donas J., Deharveng J.M., 1987, A&A 180, 12
 Engargiola G., 1991, ApJS 76, 875
 Falgarone E., Puget J.L., Péroult M., 1992, A&A 257, 715
 Fitzpatrick E.L., Massa D., 1988, ApJ 328, 734
 Garcia-Burillo S., Combes F., Gerin M., 1993, A&A 274, 148
 Garmany C.D., 1994, PASP 106, 25
 Gerin M., Casoli F., Combes F., 1991, A&A 251, 32
 Güsten R., Mezger P., 1983, Vistas in Astronomy 26, 159
 Helou G., Malhotra S., Beichman C.A. et al., 1996, A&A 315, L157
 Henyey L.G., Greenstein J.L., 1941, ApJ 93, 70
 Heydari-Malayeri M., Beuzit J.L., 1994, A&A 287, L17
 Hippelein H., Lemke D., Haas M. et al., 1996, A&A 315, L82
 Jaffe D.T., Zhou S., Howe J.E. et al., 1994, ApJ 436, 203
 Kennicutt R., 1989, ApJ 344, 685
 Klein U., Beck R., Buczylowski U.R., Wielebinski R., 1982, A&A 108, 176
 LeBourlot J., Pineau des Forêts G., Roueff E., 1993, A&A 267, 233
 Leisawitz D., 1991, ApJS 77, 451
 Leisawitz D., Hauser M.G., 1988, ApJ 332, 954
 Leisawitz D., Bash F.N., Thaddeus P., 1989, ApJS L. 70, 731
 Li, Li, 1995, A&A 301, 666
 Lord S.D., Malhotra S. et al., 1996, A&A 315, L117
 Lu N.Y., Helou G., Tuffs R. et al., 1996, A&A 315, L153
 Mc Kee C.F., Williams J.B., 1997, ApJ 476, 144
 Madden S., Geis N., Genzel R. et al., 1993, ApJ 407, 579
 Madden S., Geis N., Genzel R. et al., 1994, Infrared Phys. Technol. 35, no 2/3, 311
 Malhotra S., Helou G., Van Buren D. et al., 1996, A&A 315, L161
 Martin P., 1995, AJ 109, 2428
 Massey P., Johnson K.E., De Gioia-Eastwood K., 1995, ApJ 454, 151
 Mathis J.S., Mezger P.G., Panagia N., 1983, A&A 128, 212
 Mezger P., 1972, in *Interstellar matter*, editors W.C. Wickramasinghe, F.D. Kahn and P.G. Mezger
 Miller W.W. III., Cox D.P., 1993, ApJ 417, 579
 Murthy J., Walker H.J., Henry R.C., 1992, ApJ 401, 574
 Myers P.C., Dame T.C., Thaddeus P. et al., 1986, ApJ 301, 398
 Osterbrock D.E., 1989, in *Astrophysics of Gaseous Nebulae and Active Galactic Nuclei*, University Science Books
 Peimbert M., Rayo J.F., Torres-Peimbert S., 1975, Revista Mexicana de Astronomia y Fisica 1, 289
 Rifatto A., Longo G., Capaccioli M., 1995, A&AS 114, 527
 Rice W., Boulanger F., Viallefond F., Soifer B.T., Freedman W.L., 1990, ApJ 358, 418
 Rubio M., Lequeux J., Boulanger F. et al., 1993, A&A 271, 1
 Ryter C., Puget J.L., Péroult M., 1987, A&A 186, 312
 Seaton M.J., 1979, MNRAS 187, 73
 Shibai H., Okuda H., Nakagawa T. et al., 1991, ApJ 374, 522
 Snow T.P., Witt A., 1996, ApJ 468, L65

- Solomon P., Sanders D., Rivolo A.R., 1985, ApJ 292, L19
Thronson H.A., Majewski S., Descartes L., Hereld M., 1990, ApJ 364, 456.
Tielens A. G. G. M., Hollenbach D., 1995, ApJ 291, 747
Tuffs R., Lemke D., Xu C. et al., 1996, A&A 315, L149
Turner J.L., Ho P., 1994, ApJ 421, 122
van der Hulst J.M., Kennicutt R.C., Crane P.C., Rots A.H., 1988, A&A 195, 38
Walterbos R.A.M., Greenawalt B., 1996, ApJ 460, 696
Williams J., McKee C., 1997, ApJ 476, 166
Witt A., 1977, ApJS 35, 1
Witt A., Gordon K.D., 1996, in *Unveiling the Cosmic Infrared Background*, E. Dwek ed., AIP Conf. Proc 348
Wolfire M.G., Hollenbach D., McKee C.F., Tielens A.G.G.M., Bakes E.L.O., 1995, ApJ 443, 152
Wright E.L., Mather J.C., Bennett C.L. et al., 1991, ApJ 381, 200
Wyse R.F.G., Silk J., 1989, ApJ 339, 700
Young J., Scoville N., 1982, ApJ 258, 476
Young J., Allen L., Kenney J.D.P., Lesser A., Rownd B., 1996, AJ 112, 1903